

XMM-*Newton* and FUSE Tentative Evidence for a WHIM filament along the Line of Sight to PKS 0558-504

F. Nicastro^{1,2,3}, Y. Krongold⁴, D. Fields⁵, M.L. Conciatore³, L. Zappacosta³, M. Elvis³, S. Mathur⁶, I. Papadakis⁷

ABSTRACT

We present a possible OVIII X-ray absorption line at $z = 0.117 \pm 0.001$ which, if confirmed, will be the first one associated with a broad HI Ly β (BLB: FWHM=160 $^{+50}_{-30}$ km s $^{-1}$) absorber. The absorber lies along the line of sight to the nearby ($z = 0.1372$) Seyfert 1 galaxy PKS 0558-504, consistent with being a WHIM filament. The X-ray absorber is marginally detected in two independent XMM-*Newton* spectra of PKS 0558-504, a long ~ 600 ks Guest-Observer observation and a shorter, ~ 300 ks total, calibration observation, with a combined single line statistical significance of 2.8σ (2.7σ and 1.2σ in the two spectra, respectively). When fitted with our self-consistent hybrid-photoionization WHIM models, the combined XMM-*Newton* spectrum is consistent with the presence of OVIII K α at $z = (0.117 \pm 0.001)$. This model gives best fitting temperature and equivalent H column density of the absorber of $\log T = 6.56^{+0.19}_{-0.17}$ K, and $\log N_H = (21.5 \pm 0.3)(Z/Z_{0.01\odot})^{-1}$ cm $^{-2}$, and predicts the marginal contribution of only two more lines within the XMM-*Newton* RGS band pass, NeIX K α ($\lambda = 13.45$ Å) and FeXVII L ($\lambda = 15.02$ Å), both with equivalent widths well within the 1σ sensitivity of the combined XMM-*Newton* spectrum of PKS 0558-504 ($EW^{1\sigma} < 3$ mÅ). The lack of detection of associated OVI in the archival FUSE spectrum of PKS 0558-504, allows us to infer a tighter lower limit on the temperature, of $\log T > 6.52$ K (at 1σ).

¹Osservatorio Astronomico di Roma - INAF, Via di Frascati 33, 00040, Monte Porzio Catone, RM, Italy

²IESL, Foundation for Research and Technology, 711 10, Heraklion, Crete (Greece)

³Harvard-Smithsonian Center for Astrophysics, 60 Garden st., Cambridge, MA 02138, USA

⁴Instituto de Astronomia, Universidad Nacional Autonoma de Mexico, Mexico City (Mexico)

⁵L.A. Pierce College, 6201 Winnetka Ave., Woodland Hills, CA, USA

⁶Ohio-State University, Columbus, OH, USA

⁷Physics Department, University of Crete, P.O. Box 2208, GR-710 03 Heraklion, Crete (Greece)

The statistical significance of this single X-ray detection is increased by the detection of broad and complex HI Ly β absorption in archival FUSE spectra of PKS 0558-504, at redshifts $z = 0.1183 \pm 0.0001$ consistent with the best-fitting redshift of the X-ray absorber. The FUSE spectrum shows a broad (FWHM= 160_{-30}^{+50} km s $^{-1}$) absorption complex, which we identify as HI Ly β $z_{BLB} = (0.1183 \pm 0.0001)$. The single line statistical significance of this line is 4.1σ (3.7σ if systematics are considered). A possible HI Ly α is marginally hinted in an archival low-resolution ($\Delta\lambda \sim 6$ Å) IUE spectrum of PKS 0558-504, at a redshift of $z = (0.119 \pm 0.001)$ and with single line significance of 1.7σ . Thus, the combined significance of the three (XMM-*Newton*, FUSE, and IUE) independent tentative detections, is 5.2σ (5.0σ if the HI Ly α is not considered, and 4.6σ if the systematics in FUSE are considered).

The detection of both metal and H lines at a consistent redshift, in this hot absorbing system, allows us to speculate on its metallicity. By associating the bulk of the X-ray absorber with the BLB line detected in the FUSE spectrum at $z_{BLB} = 0.1183 \pm 0.0001$, we obtain a metallicity of 1-4% Solar.

Although the absorber is only blueshifted by ~ -6000 km s $^{-1}$ from the systemic redshift of PKS 0558-504, the identification of the absorbing gas with a high velocity nuclear ionized outflow, is unlikely. The physical, chemical and dynamical properties of the detected absorber are all quite different from those typically found in the Warm Absorber (WA) outflows, commonly detected in Seyferts and higher luminosity quasars. WA outflow velocities typically span a range of few hundreds to $\sim 1 - 2$ thousands km s $^{-1}$; WA metallicities, when measured, are typically found to be at least Solar; high-ionization WAs are virtually always found to co-exist with lower-ionization X-ray and UV phases. All this strongly suggests that the absorber, if confirmed, is an intervening WHIM system.

Subject headings: WHIM, Absorption Lines

1. Introduction

In the present epoch ($z < 1 - 2$), over half (54 %, Fukugita, 2003) of the baryons are missing. They are predicted by Big-Bang Nucleosynthesis (e.g. Kirkman et al., 2003), inferred by density fluctuations of the Cosmic Microwave Background (e.g. Bennet et al., 2003; Spergel et al., 2007), and seen at $z \sim 3$ in the “Ly α Forest” (e.g. Rauch, 1998; Weinberg et al., 1997), but by $z < 2$ they are unaccounted for in detected stars and gas (Fukugita,

2003). According to hydrodynamical simulations for the formation of structures in a Λ -CDM Universe (e.g. Cen & Ostriker, 2006), most, if not all, of these missing baryons should be in a barely visible “warm-hot” phase of the filamentary intergalactic medium (the WHIM). The WHIM was shock-heated to temperatures of $10^5 - 10^7$ K during the continued process of collapse and structure formation, and enriched up to $Z^{WHIM} = 0.1 - 1 Z_{\odot}$ by galaxy superwinds (GSW, Cen & Ostriker, 2006). These GSWs efficiently removed metals from the cool and dense ISM phase in galaxies and spread them into the tenuous ($n_e \sim 10^{-6} - 10^{-4} \text{ cm}^{-3}$, i.e. overdensities $\delta \sim 5 - 500$ compared to the average density of the Universe) WHIM phase, enriching the gas to few percent, and up to tens of percent, of the solar metallicity values (e.g. Cen & Ostriker, 2006). WHIM filaments are too tenuous to be detected through their bremsstrahlung and line emission with current X-ray instruments (e.g. Yoshikawa et al., 2003). However, integrated column densities of high-ionization metal ions along a random section of one of these filaments could reach values as high as $\sim 10^{16} \text{ cm}^{-2}$ (OVII in the soft X-Rays) and $\sim 10^{14} \text{ cm}^{-2}$ (OVI in the Far-Ultraviolet: FUV), imprinting metal absorption lines in the FUV and soft X-ray spectra of background sources with equivalent width ranging between $EW \sim 1 - 20 \text{ m}\text{\AA}$ (the OVII $K\alpha$ in the X-rays) and $EW \sim 10 - 100 \text{ m}\text{\AA}$ (the $\lambda \simeq 1032 \text{ \AA}$ transition, in the FUV).

The most intense of these absorption lines are the $\text{OVI}_{1s^22s \rightarrow 1s^22p}$ doublet in the UV ($\lambda = 1031.926, 1037.617 \text{ \AA}$), and the CV $K\alpha(r)$ ($\lambda = 40.268 \text{ \AA}$), OVII $K\alpha(r)$ ($\lambda = 21.602 \text{ \AA}$), CVI $\text{Ly}\alpha$ ($\lambda = 33.74 \text{ \AA}$) and OVIII $\text{Ly}\alpha$ ($\lambda = 18.97 \text{ \AA}$), in the X-ray band. Which of these lines dominates, depends on the ionization state of the gas, that is mainly on its temperature (and at a second order on the gas volume density). Davé and collaborators (2001) showed that the baryon temperature distribution in the intergalactic space, peaks at $\log T \sim 6.6$ K, and is strongly skewed toward low temperatures: 50% of the baryon in the WHIM are found between $\log T = 5.6$ K and $\log T = 6.7$ K at a weighted average temperature of $\log T = 5.9$ K, while the low ($\log T = (5 - 5.6)$ K) and high ($\log T = (6.6 - 7)$ K) temperature tails of the WHIM temperature distribution, contain 27% and 23% of the gaseous baryons in the Universe, respectively, around weighted average temperatures of $\log T = 5.4$ K and $\log T = 6.7$ (Conciatore et al., in preparation). So, while the vast majority (73%) of the baryons in the WHIM should absorb and emit in the X-rays at the wavelengths of the He-like (50%) and/or H-like (23%) ions of C and O, a substantial fraction of the WHIM (27%) should be detectable in the FUV, through Li-like C and O transitions.

These theoretical predictions have been confirmed by FUV observations (e.g. Danforth & Shull, 2005, 2008; Tripp et al., 2008; Richther, 2006). Danforth & Shull (2005) analyzed FUSE data of 31 AGNs with $z < 0.15$ to search for OVI absorption counterparts to 129 known $\text{Ly}\alpha$ absorbers. They found 40 such systems, deriving a $dN_{\text{OVI}}/dz (\geq EW_{\text{Thresh}})$ that agrees strikingly with the latest predictions by Cen & Fang (2006; see their Fig. 2).

However, as pointed out recently by Tripp et al. (2008), the vast majority of the associated HI Ly α absorption lines are too narrow to be produced in gas with typical WHIM temperatures. Danforth & Shull (2008) proposed that low-ionization metals and narrow HI Ly α trace mildly photoionized medium (the low- z Ly α Forest: $\sim 30\%$ of the baryons), while narrow-HI/OVI/NV associations trace a multiphase intergalactic medium, with a photoionized portion of the intervening filament imprinting the narrow-HI absorption and a shock-heated part (WHIM) imprinting the OVI/NV on the UV spectra ($\sim 10\%$ of the baryons). Danforth & Shull (2008) estimate $\Omega_{WHIM}^{OVI} = 0.34\%$ (down to $\log N_{OVI} > 13.4 \text{ cm}^{-2}$). This is $\sim 15\%$ of the “missing mass” (strictly speaking, only a lower limit, given the large uncertainties in the ionization correction for the OVI-bearing gas), in good agreement with the WHIM baryon fraction predicted to reside in the low-temperature tail of the WHIM mass-temperature distribution.

Detecting the bulk of the ‘Missing Baryons’ in the “X-Ray Forest”, instead, has proven to be extremely difficult. This is because of the unfortunate combination of (a) the still limited resolution ($R \sim 400$ at $\lambda = 21.6 \text{ \AA}$) and the low throughput ($A_{Eff} \sim 20 - 40 \text{ cm}^2$) of the current high-resolution X-ray spectrometers [the XMM-*Newton* Reflection Grating Spectrometer (RGS, den Herder, et al. 2001) and the *Chandra* Low Energy Transmission Grating (LETG: Brinkman et al., 2000)]; (b) the lack of bright ($f_{0.5-2keV} \geq 10^{-11} \text{ erg s}^{-1} \text{ cm}^{-2}$) extragalactic point-like targets (e.g. Conciatore et al., in preparation); and, (c) the dramatic steepening ($\Delta\alpha \gtrsim 1.5$) of the predicted number density of metal WHIM filaments per unit redshift at ion column densities $\gtrsim 10^{15} \text{ cm}^{-2}$.

Current evidence is still limited, and highly controversial: in 2005, Nicastro et al. (2005a,b) reported the first two $\geq 3\sigma$ detections of absorption systems identifiable with WHIM filaments, at $z = 0.011$ and $z = 0.027$, towards the blazar Mkn 421, which was in outburst. One of these two systems is at a redshift consistent with that of a known intervening HI Ly α absorber (Shull, Stocke & Penton, 1996) that line, however, is too narrow, and so the absorbing gas too cold, to be physically associated with the X-ray metal filament. This claim has been questioned in two subsequent papers by Kaastra et al. (2006) and Rasmussen et al. (2007), based on: (a) apparent wavelength inconsistencies for some of the lines, which called into question their association with a given WHIM system; (b) statistical arguments for a significantly lower detection significance for the WHIM identifications than originally reported by Nicastro et al. (2005a,b); and (c) the lack of detection of these two systems in XMM-*Newton* RGS calibration spectra of Mkn 421 (but see also Nicastro, Mathur & Elvis, 2008, for rebuttal arguments). Fang, Canizares & Yao (2007) proposed the detection of an OVIII WHIM filament along the line of sight to the blazar PKS 2155-304, once again near the redshift of a known narrow HI Ly α absorber not due to the same gas as the putative X-ray filament, because of the line width. The above reported pieces of evidence for the exis-

tence of an “X-ray Forest” at low redshift, have been gathered by exploiting the technique of observing random lines of sight toward the brightest possible X-ray sources, with exposures long enough to reach extremely high S/N spectra. This technique has the advantage of not being biased toward the strongest WHIM systems, and so allows probes of the bulk of the WHIM mass distribution. However, the WHIM is predicted, and in the FUV has most likely been found (e.g. Stocke et al., 2006b), to correlate strongly with galaxy concentrations in the Universe: the densest of such concentrations are also supposed to host the nodes, and so the densest and hottest parts, of the WHIM network.

An alternative technique, therefore, is to target the WHIM search in the X-rays along those lines of sight toward bright background X-ray sources that intercept large scale structure concentrations. By exploiting this technique Buote et al. (2009), reported a $\sim 3\sigma$ detection of a high column density ($N_{OVII} \geq 10^{16} \text{ cm}^{-2}$) OVII $K\alpha$ absorption line, along the line of sight to the blazar H 2356-309, at the redshift of a very large concentration of galaxies in the Sculptor Wall. This technique has the disadvantage of probing only the extreme high-temperature/density and low-mass fraction ends ($\sim 23\%$) of the WHIM distribution.

All the above proposed WHIM detections so far, suffer the serious handicap of lacking the detection of a clearly associated HI counterpart. The detection of broad HI Lyman lines (mostly $\text{Ly}\alpha$ at $\lambda = 1215.67 \text{ \AA}$ - BLA - and $\text{Ly}\beta$ at $\lambda = 1025.72 \text{ \AA}$ - BLB) is vital for a proper assessment of the WHIM metallicity and mass, and require the use of both X-ray and FUV facilities. Without HI, metallicity cannot be determined and so a cosmological mass density Ω_b^{WHIM} cannot be derived.

The expected thermal FWHM of an absorption line imprinted from a gas of particles of mass m at the equilibrium temperature T , is given by $2\sqrt{2\ln 2}$ times the variance of the velocity distribution (the Doppler parameter b), that is $\text{FWHM} = 2\sqrt{2\ln 2}\sqrt{kT/m}$. For HI, this implies a broadening of $\text{FWHM} \sim 380 \text{ km s}^{-1}$ at $\log T = 6.5$ ¹.

The HI fraction, relative to the total H, in gas with temperatures in the $\log T = (5.8 - 6.3)$ range (where 50% of the WHIM should be, e.g. Davé et al., 2001), spans the interval $10^{-6.2} - 10^{-7.2}$. Thus only very shallow ($\text{EW}(\text{Ly}\alpha) \simeq 8 - 80 \text{ m\AA}$) and broad HI absorption lines are expected to be imprinted onto FUV spectra by WHIM filaments, requiring spectra with $\text{S/N} \simeq 10 - 100$ per resolution element to make them detectable.

Here we present the first tentative detection of a hot (X-ray) WHIM filament along the line of sight to the $z = 0.1372$ Seyfert galaxy PKS 0558-504, that is physically associated with

¹For heavier elements, the width scales with the inverse of the root square of the atomic weight. So, for example, for O, Ne and Fe, at $\log T = 6.5$, $\text{FWHM} = 95, 85$ and 51 km s^{-1} .

a BLA HI absorber. A full band analysis of the XMM-*Newton* RGS spectrum of PKS 0558-504, is deferred to a companion paper (Papadakis et al., 2009, submitted). In §2 we present the XMM-*Newton*, FUSE and IUE data that we use in our analysis. §3 and 4 are dedicated to the X-ray and FUV data reduction and analysis. In §5 we critically discuss our findings, and in §6 we summarize our conclusions.

2. XMM-*Newton*, FUSE and IUE Data of PKS 0558-504

Between February 2000 and October 2001, PKS 0558-504 was the subject of an extensive calibration campaign with XMM-*Newton*, with a total exposure of 312 ksec (hereinafter ‘CAL spectrum’). More recently, in September 2008, PKS 0558-504 was re-observed by the XMM-*Newton* for 618 ksec, as part of an approved cycle 8 Guest Observer program (PI. S. Papadakis; hereinafter ‘GO spectrum’). In this work we make use of the RGS spectra extracted from both data sets. We focus mostly on the analysis of the longer and much higher S/N 2008 (16 vs 9, at 25 Å) GO spectrum. We use the lower S/N 2000-2001 CAL spectrum for consistency checks.

PKS 0558-504 was observed by the FUSE satellite twice: on 1999, December 10 and 2001, November 7, with net exposure times of 47.2 ksec and 48.3 ksec, respectively. In our analysis we co-add the two spectra from the Lif2A channel (with the highest efficiency in the 1100-1200 Å interval) to maximize the S/N and perform our search for intervening BLAs and BLBs in this co-added FUSE spectrum ².

Finally, PKS 0558-504 has been observed three times with the ‘Short-Wavelength’ spectrometer of the IUE satellites (the only one covering the wavelength range of interest), on 1987, September 22, and 1989, November 14-15. In our analysis we use the highest S/N of the three spectra (with a net exposure time of 16.2 ksec), the one taken on 1989, November 15, and check the other two spectra for consistency.

Table 1 lists the journal of the XMM-*Newton*, FUSE and IUE observations used in this work. For all our spectral fitting we use the fitting package *Sherpa*, of the Chandra Interactive Analysis of Observation (*Ciao*) software (v. 4.1.2; Freeman, Doe & Siemiginowska, 2001).

²We also reduced and analyzed the sum of the two spectra from the Lif1B channel, which is sensitive (though with about half of the effective area of the Lif2A channel) in a wavelength interval similar to that of the Lif2A. However, the Lif1B channel is unreliable at $\gtrsim 1140$ Å (The FUSE Data Handbook, Chapter 7, §7.3.2, http://archive.stsci.edu/fuse/DH_Final/Factors_Affecting_FUSE_Data.html), which is the region of interest for our analysis. Therefore we decided to consider only the Lif2A channel in our analysis (but see also footnote 9, §4).

3. The RGS Spectrum of PKS 0558-504

3.1. RGS Data Reduction and Analysis

The 2008 GO RGS data of PKS 0558-504 were reduced as in Papadakis et al. (2009), and the same standard reduction procedure was applied to the 2000-2001 calibration observations of this target. The data were cleaned for periods of high background activity, by excluding events taken within time-intervals where the background deviated positively by its average level by more than 2σ . Finally RGS1 and RGS2 spectra and responses of the single observations of the two datasets (CAL and GO) were co-added and averaged by using the *rgscombine* tool. This produced total net exposures of 480 ksec (RGS1) and 466 ksec (RGS2), for the GO dataset, and 309 ksec (RGS1) and 283 ksec (RGS2) for the CAL dataset. Despite a 30% higher average flux level of PKS 0558-504 during the CAL observations, compared to the GO observations, and a relatively small difference of only 65% in the net exposure times of the two datasets, the S/N of the GO spectra is significantly (factor of ~ 2) higher than that of the CAL spectra. In half RGS resolution element ($30 \text{ m}\text{\AA}$), at 0.5 keV the co-added RGS1 CAL spectrum has S/N=9, compared with S/N=16 for the GO spectrum. This difference in S/N is due to the much higher (more than an order of magnitude) level of the average background during all individual CAL observations, compared with the GO observations. This is clearly seen in Figure 1, where we plot the combined GO RGS1 20-24 \AA background-subtracted source (green filled circles and errorbars) and background (blue filled circles and errorbars) spectra of PKS 0558-504, together with the combined CAL RGS1 20-24 \AA background-subtracted source (black empty squares and errorbars) and background (red empty squares and errorbars) spectra of PKS 0558-504. We therefore decided not to further combine the RGS spectra of the two datasets, and to analyze them separately and simultaneously.

In our spectral analysis we bin the RGS spectra two $45 \text{ m}\text{\AA}$ bin (about half the nominal FWHM resolution of the RGSs).

3.2. X-Ray Spectral Fitting

In our companion paper (Papadakis et al., 2009), we present the broad-band 0.4-2 keV spectral analysis of the 2008 RGS spectra of PKS 0558-504, and show that the soft X-ray continuum of PKS 0558-504 is well modeled by a broken power law with a break energy of $E_{brk} \sim 1.5 \text{ keV}$, attenuated by Galactic ISM absorption. More importantly we exclude the presence of a Warm Absorber with typical column densities and ionization parameters (Papadakis et al., 2009). This is consistent with the absence of associated, intrinsic, Narrow

Absorption Lines (NALs) in the Far Ultraviolet spectrum of PKS 0558-504 (Dunn et al., 2007). However, Papadakis et al. (2009) also note that weak absorption line-like features are detected in the spectrum of PKS 0558-504, in the narrow 20-24 Å spectral interval. These three lines, and in particular the line at $\lambda = 21.18$ Å are the subject of this study.

We first explored the 20-24 Å region of the GO and CAL RGS1 spectra of PKS 0558-504 (the RGS2 is blind in this wavelength range, due to the lack of a read-out CCD chip). We fitted the data simultaneously, with two local continuum models, each including a power law attenuated by neutral absorption with the metallicity set to Anders & Grevesse (1989). While such a model gives a statistically acceptable fit for the GO spectrum of PKS 0558-504, it leaves broad and systematic residuals in the CAL spectrum. This is because the *rgscombine*-averaged CAL response matrix fails to properly reproduce the depth of the several effective area features present in this portion of the RGS1 spectrum. We therefore added a number of $\text{FWHM} \sim 0.5 - 1$ Å broad emission and absorption Gaussians to the best fitting continuum model of the CAL spectrum of PKS 0558-504, until we reached a statistically acceptable fit. Three narrow regions with a deficit of counts are left in the GO and CAL residuals to the best fitting continuum models, at $\lambda \sim 23.5$ Å, $\lambda \sim 21.6$ Å and $\lambda \sim 21.2$ Å. To model these residuals we added three Gaussians to our best-fitting continuum models and refitted the data leaving all Gaussians parameters free to vary independently in the fit to the GO spectrum, but linking the line energies and Gaussian widths in fitting the CAL spectrum to those of the corresponding parameters of the fitting model of the GO spectrum. The first three rows of Table 2 show the best fitting parameters of these three absorption lines. Errors on wavelengths and redshifts are assumed to be equal to 1 bin-size, 30 mÅ, if unresolved by the fitting routine). Figure 2 shows the 20-24 Å RGS1 CAL and GO data of PKS 0558-504, with their best-fitting models superimposed. The first two of these lines, at $\lambda = 23.52 \pm 0.03$ Å and $\lambda = 21.61 \pm 0.03$ Å, are easily identified with the $K\alpha$ inner shell transition from atomic OI in the Interstellar Medium of the Galaxy, and the $K\alpha$ He-like transition from OVII either in our Galaxy halo or in the Local group (e.g. Bregman et al., 2007 and references therein). The third line, at $\lambda = 21.17 \pm 0.04$ Å, appears marginally resolved (but still consistent with an unresolved Gaussian at a 1σ confidence level ³) in the RGS1 ($\text{FWHM} \lesssim 1200$ km s⁻¹: Table 2) and has no obvious identification with transitions at $z \simeq 0$. If red-shifted to the systemic redshift of PKS 0558-504 ($z = 0.1372$, REFs), this line would have a rest-frame wavelength of $\lambda = 18.62$ Å, close to the rest-frame wavelength of the OVII $K\beta$ transition.

³the *projection* routine in Sherpa, which we use here to compute uncertainties and upper limits, finds only an upper limit for the line FWHM, at a 1σ confidence level. This is because of the high non-gaussianity of the RGS Line Spread Function (e.g. Williams et al., 2005), which makes the effective LSF FWHM significantly broader than the nominal Gaussian equivalent LSF FWHM of 60 mÅ (corresponding to ~ 900 km s⁻¹ at 21.2 Å).

However, in this case, a much stronger (factor ~ 6.4) OVII $K\alpha$ line ⁴ with $EW \sim 60 \text{ m}\text{\AA}$ should be visible at $\lambda = 24.55 \text{ \AA}$. Such a line is not seen in the data (see also Papadakis et al., 2009) at a 3σ limit of $EW < 18 \text{ m}\text{\AA}$ ⁵. Moreover, the absence of intrinsic OVI absorption in the FUSE data of PKS 0558-504 (Dunn et al., 2007), makes this interpretation less likely.

The next possible identification is with an intervening absorber, between the redshift of PKS 0558-504 and us. This imposes the condition that the line has a rest-frame wavelength in the 18.6-21.2 \AA spectral interval. The strongest resonant absorption line expected in this spectral range is the OVIII $\text{Ly}\alpha$ transition, with an unresolved doublet at an oscillator strength weighted average wavelength $\langle \lambda \rangle = 18.97 \text{ \AA}$. This would give a redshift of $z = 0.116 \pm 0.002$ for the intervening absorber.

3.3. Consistency Test with a Self-Consistent WHIM Spectral Model

To check whether the presence of an OVIII $_{K\alpha}$ WHIM filament at $z = 0.116 \pm 0.002$ along the line of sight to PKS 0558-504, is consistent with the full band XMM-*Newton* RGS spectra of this target, we used our hybrid ionization (collisional + photoionization by the meta-galactic UV and X-ray background at a given redshift) WHIM spectral models (an evolution of our PHotoinized Absorber Spectral Engine - “PHASE” -, Krongold et al., 2003), to simultaneously fit the RGS1 and RGS2 Cal and GO data of PKS 0558-504. The fitting model includes our best-fitting continuum model (a combination of power-laws and broad gaussians to cure residual calibration uncertainties), two negative gaussians to model the OI $_{K\alpha}$ and OVII $_{K\alpha}$ absorptions at $z \simeq 0$, and a WHIM model. In the X-ray band alone one cannot constrain the absolute metallicity of the absorber (for which detection of HI is needed), since the ionization balance of an hybridly ionized cloud of gas (i.e. the fractional ion abundances), parameterized by the temperature of the absorber, at equilibrium, is virtually independent on metallicity (see also §5.2). Thus, for fitting purposes only, we froze the WHIM metallicity to Solar. The turbulent velocity of the absorber was frozen to 400 km s^{-1} (about 1/2 of the RGS FWHM resolution at 22 \AA). In a hybrid-ionization WHIM model, photoionization by the meta-galactic UV and X-ray photon field, is only a secondary ionization mechanism, and its relative importance, compared to the collisional shock mechanism, depends only on

⁴together with several other strong lines from He- and H-like ions of C, N and Ne

⁵we also caution, however, that although the RGS1 spectra of PKS 0558-504 are free of instrumental feature at, exactly, 24.55 \AA , this spectral region of the RGS1 contains several instrumental features, which might reduce, due to calibration uncertainties, the true sensitivity of the RGS1 spectrum at 24.55 \AA . See also §5.2

the volume density of the WHIM filament: the lower the density the more important the photoionization contribution. In such models the absorber density is thus highly degenerate with the absorber temperature and equivalent H column density, and so is difficult to constrain. We therefore froze the density of the absorbing gas to a typical expected WHIM value of $n_b = 10^{-5} \text{ cm}^{-3}$ (overdensity $\delta \simeq 50$ compared to the average baryon density in the Universe), corresponding to an ionization parameter (the ratio between the photon density at the surface of the absorbing cloud and the baryon density in the cloud) of $\log U = -1.9$ at $z = 0.1$. At such densities (and higher), the photoionization contribution is essentially negligible, and the model reduces to a pure collisional ionization model. The remaining WHIM parameters, namely the gas temperature and equivalent hydrogen column density, and the redshift of the WHIM filament, were left free to vary in the fit. The best-fitting WHIM model (Fig. 3, black curve) has $\log T = 6.56_{-0.17}^{+0.19}$, $\log N_H = 19.5 \pm 0.3$ (for $Z = Z_\odot$) and $z = 0.117 \pm 0.001$. This model fits the most prominent OVIII $K\alpha$ line at $z = 0.117$, and predicts only two additional weak absorption lines ($EW \lesssim 1 \text{ m\AA}$): the NeX $K\alpha$, at $\lambda = 15.02 \text{ \AA}$ (WHIM filament frame) and a strong (oscillator strength 2.95) FeXVII L line at $\lambda = 16.77 \text{ \AA}$ (Fig. 3, black curve).

Figure 4, 5 and 6 shows the two portions of the RGS CAL and GO spectra of PKS 0558-504, in which the lines predicted by the best-fitting WHIM model lie. The superimposed red curve is the best fitting WHIM model convolved with the instrumental responses. The OVIII $K\alpha$ line is detected both in the CAL and GO spectra (Fig. 4). The position of the predicted NeIX $K\alpha$ and FeXVII L lines is marked in Fig. 5 (RGS1 and RGS2 GO spectra of PKS 0558-504) and Fig. 6 (RGS1 and RGS2 CAL spectra of PKS 0558-504): the strength of these lines is $< 1/3$ the minimum detectable 1σ EW in the combined CAL+GO spectrum (Table 2). We note the hint of the presence of the FeXVII L line at 16.77 \AA in both the RGS1 GO (Fig. 5, top panel) and RGS2 CAL (Fig. 6, bottom panel) spectra of PKS 0558-504.

In Figure 3 we plot the best fitting WHIM model (central, black curve) together with its negative (lower, red curve) and positive (upper, blue curve) 1σ temperatures. Both lower and upper limits on the temperature are weak. The strongest X-ray lower limit diagnostics in the model is the increasing strength of OVII K series absorption lines. However, the sensitivity of the RGS1 GO and CAL spectra of PKS 0558-504 at the wavelength of the strongest line of this series (the OVII $K\alpha$ line) is dramatically reduced by the presence of an instrumental feature due to a bad pixel in the read out dispersion detectors. On the other end, at higher temperature, the limit is set by the decrease of opacity at the wavelengths of the OVIII $K\alpha$ transitions, which is only detected at a combined single-line significance level of 2.8σ in the data. This can be also seen in Figure 7, where we show the 68%, 90% and 95% $\log T - \log N_H$ contours of the best-fitting WHIM model. The parameters are clearly correlated and the temperature poorly constrained both at low and high temperatures. However, low

temperatures and high column densities are excluded at high confidence levels.

4. The FUSE and IUE Spectra of PKS 0558-504

We searched the The Multimission Archive at STsci (MAST) archive ⁶ for FAR-UV data of PKS 0558-504 and found several data sets, taken with FUSE, HST and IUE satellites (Table 1). Our main goal was to search for HI ($\text{Ly}\alpha$ and $\text{Ly}\beta$) and OVI absorption either at or near the systemic redshift of PKS 0558-504, or at a redshift consistent with that of the putative X-ray WHIM filament, tentatively detected in the RGS spectrum of PKS 0558-504. The available archival HST spectrum of PKS 0558-504 was taken with the STIS-G230 gratings, and so covers a wavelength interval ($\lambda = 2760 - 2910 \text{ \AA}$) not relevant to this analysis. The FUSE and IUE spectra, instead, cover two important regions: (a) the HI $\text{Ly}\beta$ and OVI regions (FUSE) and (b) the HI $\text{Ly}\alpha$ region (IUE). We retrieved these data sets from the MAST archive, and analyzed them to search for a secure identification of the X-ray absorber.

FUSE observed PKS 0558-504 twice, in two different programs (P101, Sembach 1999, and C149, Prochaska 2002). All FUSE observations after the end of operations were re-reduced using the final version of the CalFUSE pipeline (v3.2.3, Dixon et al., 2007), and we used the resultant science calibrated files. We used specific IRAF scripts ⁷ to co-add the data from the Lif 2A channel, which covers the wavelength range 1087-1181 \AA , with a total exposure time of 90.3 ks. The spectrum was then binned to two different resolutions: the natural resolution of FUSE (3 bins; 11 km/s) and a poorer resolution (20 bins; 70 km/sec) with higher S/N per bin, specifically to search for broad, shallow absorption features.

We use the fitting package *Sherpa* in Ciao (v. 4.1.2; Freeman, Doe & Siemiginowska, 2001), to search the FUSE spectrum for: (a) AGN intrinsic absorption between -1000 and +1000 km s^{-1} of the systemic redshift of PKS 0558-504; (b) intervening absorption at a redshift consistent with that of the putative X-ray WHIM filament. Specifically, for each of the two possible systems, we searched for absorption lines from: (1) the NIII triplet at $\lambda = 989.80 \text{ \AA}$, $\lambda = 991.51 \text{ \AA}$, and $\lambda = 991.57 \text{ \AA}$; (2) the OVI doublet at $\lambda = 1031.93 \text{ \AA}$ and $\lambda = 1037.62 \text{ \AA}$; and (3) the HI $\text{Ly}\beta$, at $\lambda = 1025.72 \text{ \AA}$. We confirm the non-detection of intrinsic (i.e. nuclear) ionized or neutral absorption, down to $EW \lesssim 30 \text{ m\AA}$ (3σ) of Dunn et al. (2007). However, we do detect several absorption lines in the wavelength range 1137-

⁶<http://archive.stsci.edu/index.html>

⁷http://fuse.pha.jhu.edu/analysis/IRAF_scripts.html

1155 Å (Figure 8). The strongest of these lines are easily identified as Galactic FeII, PII and possibly H2 transitions. These lines are all relatively narrow, with typical FWHM $\simeq 50 - 70$ km s⁻¹ ⁸, and exhibit two velocity components at $v_1 \simeq 0$ and $v_2 \simeq +200$ km s⁻¹ (for the low-ionization atomic transitions) ⁹, and $v_1 \simeq 0$ and $v_2 \simeq +70$ km s⁻¹ (for the molecular transition: Wakker, 2006): Figure 8.

However, we also detect a broader absorption complex at the centroid wavelength of $\lambda = 1147.1$ Å, and at single-line statistical significances of 4.1σ (Figure 8) ¹⁰. We model this absorber with a negative Gaussian, and list its best-fitting parameters and equivalent width in Table 1 ¹¹.

This absorption line is broad (FWHM = 160_{-30}^{+50} km s⁻¹) and cannot be identified with any strong Galactic transition. We identify this absorber as a broad HI Ly β (BLB) at $z_{BLB} = (0.1183 \pm 0.0001)$. The X-ray redshift of the OVIII K α absorber is consistent with z_{BLB} . At the best fitting X-ray temperature of $\log T = 6.56$ K, the thermal speed of protons is $\sqrt{2}b = 250$ km s⁻¹ and so the expected broadening of HI absorption lines is FWHM $\simeq 400$ km s⁻¹. The width of the z_{BLB} HI absorber is marginally consistent, at a 2.5σ level, with the expected broadening (Fig. 9). Here we therefore assume that the HI BLB is associated with the bulk of the X-ray OVIII absorber.

There is no detectable OVI or NIII absorption associated with the z_{BLB} HI absorber. The non-detection of OVI puts a much more stringent lower limit on the temperature of the detected WHIM filament. At the best fitting X-ray temperature the relative fraction of OVI, $\xi_{OVI} = 2.0_{1.8}^{+9.0} \times 10^{-4}$, predicts (for unsaturated lines) $EW(OVI) = 7.6_{-6.8}^{+40.6}$ mÅ. From the

⁸With the exception of the high velocity component of the FeII($\lambda 1144.94$) absorber, at $\lambda = 1145.7$ Å, for which we measure FWHM = (100 ± 40) . This absorber could be at least partly contaminated by intervening HI Ly β absorption at $z = (0.1170 \pm 0.0001)$, i.e. still consistent with the X-ray redshift of the putative OVIII intervening absorber, and so possibly representing a second HI component associated with this hot intervening WHIM filament.

⁹There are also two known velocity components in high-ionization OVI Galactic (or Galactic halo) absorption, along the line of sight to PKS 0558-504, in the velocity ranges $-115 - +135$ km s⁻¹ (Savage, 2003) and $+210 - +315$ km s⁻¹ (Sembach et al., 2003).

¹⁰The associated 1σ error here, and anywhere else in the paper, is only statistical. By taking into account the vagaries of continuum placement and fixed-pattern noise in the Lif2A FUSE spectrum of PKS 0558-504, we estimate an additional 14% systematic 1σ uncertainty. This would reduce the significance of the broad line at $\lambda = 1147.1$ Å, from 4.1σ to 3.7σ .

¹¹We note that this line is also clearly visible in the co-added Lif1B spectrum, with a slightly larger, but consistent, EW. However, due to the unreliability of the Lif1B channel at $\lambda \gtrsim 1140$ Å (see footnote 1, §2), we conservatively decided not to consider this as a supporting evidence.

FUSE data we have $\text{EW}(\text{OVI})_{z=0.118} \lesssim 12 \text{ m}\text{\AA}$ at a 1σ confidence level (Table 2). By linearly interpolating between expected OVI fractions and EWs, we derive the 1σ upper limit on the fraction of OVI corresponding to the measured $\text{EW}(\text{OVI})$ upper limit, and from this the 1σ lower limit on the temperature of the absorber. This gives: $\log T > 6.52$. Thus by combining the UV and X-ray constraints on the temperature of the WHIM filament, one gets $\log T = 6.56^{+0.17}_{-0.04}$ (Table 3).

The IUE satellite observed PKS 0558-504 twice with the ‘Short Wavelength Primary’ (SWP), low-resolution ($\Delta\lambda = 6 \text{ \AA}$) spectrometer, on 1987 September 22, and 1989, November 14-15. We retrieved the data products of these three observations from the MAST archive¹², and analyzed them with *Sherpa* (v. 4.1.2¹³; Freeman, Doe & Siemiginowska, 2001). The three SWP Low-Resolution spectra (LR) of PKS 0558-504, are dominated by the intrinsic nuclear AGN continuum and emission line spectrum. However, the two spectra with highest S/N (obsid 37589 and 37604; Table 1) show also marginal evidence for a narrow absorption feature imprinted on the blue wing of the HI Ly α broad emission line of PKS 0558-504, at $\lambda \sim 1360 \text{ \AA}$ (Figure 10). We fitted the three spectra simultaneously with a model, consisting of a powerlaw plus narrow and broad components of the HI Ly α and NV AGN emission lines and a negative absorption line to model the absorption feature at $\lambda \simeq 1360 \text{ \AA}$. The best-fitting parameters for this absorption line are listed in Table 2. We tentatively identify this low-significance (1.7σ) absorber as an intervening broad HI Ly α (BLA) at $z_{BLA} = 0.119 \pm 0.001$, a redshift consistent with that of the z_{BLB} HI absorber detected by FUSE. Figure 10 shows a portion of the highest S/N 1989 IUE-SWP LR (obsid 37604) spectrum of PKS 0558-504, with our best-fitting superimposed, and the residuals after subtracting the Gaussian at $\lambda = 1360 \pm 1 \text{ \AA}$.

4.1. Summary of the Observational Evidence

The Far-UV and X-ray spectra of PKS 0558-504 show evidence for complex absorption, which is unlikely to be intrinsic to the AGN itself (§5.1). Figure 11 summarizes these conclusions, by showing the residuals (in σ), in velocity space, to the best fitting continuum models to the FUSE (top panel), IUE-SWP LR (1989; second panel from the top) and XMM-*Newton* (GO: 3rd and 5th panels from the top; CAL: 4th panel from the top) spectra of PKS 0558-504. The residuals are centered around the absorption lines that we identify as HI Ly β , HI Ly α , OVIII Ly α and FeXVII L ($\lambda = 15.015 \text{ \AA}$, rest frame), at a mean common

¹²<http://archive.stsci.edu/index.html>

¹³<http://cxc.harvard.edu/ciao/index.html>

redshift of $z = 0.118 \pm 0.001$ (all lines are consistent with this redshift). The red arrows in the figures indicate the best-fitting centroid of each line in their respective spectra.

The FeXVII L $\lambda = 15.015 \text{ \AA}$ line (bottom panel) is only seen at 1.5σ and 2σ in the RGS1 GO and RGS2 CAL spectra (Figs. 5 and 6), and is not visible in either the RGS2 GO or in the RGS1 CAL spectra, although all data are consistent with the presence of this line at the strength predicted by the best-fitting WHIM model. The OVIII $K\alpha$ line is present both in the GO (3rd panel from the top) and CAL (4th panel from the top) RGS1 spectra (the RGS2 is blind in this spectral region). Finally, possible HI lines are seen both in the FUSE (top panel) and IUE-SWP LR spectra: a BLB is detected in the high resolution FUSE spectra, at redshifts $z_{BLB} = (0.1183 \pm 0.0001)$, and an unresolved BLA is hinted in the IUE spectra at $z_{BLA} = (0.119 \pm 0.001)$. Both redshifts are consistent with that of the X-ray absorbers, within their 1σ uncertainties. Finally we note that the measured ratio $EW_{BLA}/EW_{BLB} = (15 \pm 10)$, between the equivalent width of the low-significance BLA line (IUE) and the BLB line (FUSE) is consistent, within the large statistical errors, with the predicted value of $(EW_{HI})_{Ly\alpha}/(EW_{HI})_{Ly\beta} \simeq 7.4$, for unsaturated lines¹⁴.

The combined statistical significance of this detection is 5.2σ (4.6σ if systematics are considered, and the small contribution from the putative HI BLA is not included).

5. Discussion

5.1. Ruling Out Intrinsic Absorption

The Far-UV and X-ray absorber along the line of sight to PKS 0558-504, is only $\sim -6000 \text{ km s}^{-1}$ from the systemic redshift of PKS 0558-504. In principle, then, it could be identified with a high-velocity outflow ejected from the Seyfert’s nuclear region in the direction of our line of sight. Such phenomena are common in AGNs, and are known with the name of “Warm Absorbers (WAs, in X-rays: e.g. George et al. 1998; Piconcelli et al., 2005) or “Narrow Absorption Line” absorbers (NALs, in the UV: e.g. Crenshaw, Kraemer & George, 2003). However, we note that, the physical, chemical and dynamical properties of the detected absorber are all quite different from those typically found in WAs and NALs, commonly detected in Seyferts and higher luminosity quasars.

¹⁴For unsaturated lines, the equivalent width ratio of two electronic transitions 1 and 2 from the same series of the same ion X^i , is linearly related to the product between their oscillator strength (f) ratio times the square of their rest-frame wavelength (λ) ratio: i.e. $(EW_{X^i})_1/(EW_{X^i})_2 \simeq (f_{X^i})_1/(f_{X^i})_2 \times (\lambda_1/\lambda_2)^2$. Thus, for the $Ly\alpha$ and $Ly\beta$ transitions of HI, one expects: $(EW_{HI})_{Ly\alpha}/(EW_{HI})_{Ly\beta} \simeq 7.4$.

WA/NAL outflow velocities typically span a range of few hundreds to few thousand km s^{-1} , with $\gtrsim 80\%$ of the objects having $v_{out} \lesssim 1500 \text{ km s}^{-1}$ (e.g. Blustin et al., 2005 for WAs in X-rays, and Kriss, 2002 Crenshaw, Kraemer & George, 2003 for NALs in the UV) and are normally found to be present in several physical (temperature, and densities) and velocity components in a single object both in X-rays (e.g. Krongold et al., 2003, 2005, 2009) and in the UV (e.g. Kriss, 2002; Crenshaw, Kraemer & George, 2003). Here we measure an extreme velocity outflow of -6000 km s^{-1} and do not detect any other X-ray or FUV systems at lower velocity. The existence of very high ionization (FeXXV and FeXXVI) X-ray outflows, with sub-relativistic (i.e. $\sim 0.1c$) outflow velocities has been recently proposed for few objects (Reeves et al., 2009, and reference therein), but the existence and identification of these features are still highly debated (e.g. Uttley, 2009). In all such proposed cases, however, the high-ionization absorber has very high equivalent hydrogen column density ($few \times 10^{23} \text{ cm}^{-2}$), is seen often together with other lower velocity, lower ionization components, and in some cases requires super-solar Fe abundance (Reeves et al., 2009 and references therein). We checked the high S/N XMM-Newton GO EPIC spectrum of PKS 0558-504 for the presence of blue-shifted He- or H-like Fe absorption, and did not find any down to an equivalent hydrogen column densities of $\gtrsim 10^{21} \text{ cm}^{-2}$.

WA metallicities, when measured, are typically found to be at least Solar (e.g. Fields et al., 2005, 2007), in sharp contrast with the 1-5% Solar value we measure for this absorber. We stress that our metallicity estimate for the $z = 0.118 \pm 0.001$ absorber is virtually model-independent. The HI fractions in purely photoionized or collisionally ionized clouds of gas that best-fit the RGS spectra of PKS 0558-504, are almost indistinguishable from the HI fraction that we derive from our best-fitting hybrid-ionization WHIM models. So, the metallicity-correction needed to reconcile the HI BLB (FUSE) and BLA (IUE) column density measurements with the X-ray equivalent hydrogen column density estimate, is independent on the model used to fit the X-ray data.

Finally we stress that high-ionization WAs are virtually always found to co-exist with lower-ionization phases (e.g. HIP and LIP, Krongold et al., 2003, Andrade-Velasquez et al., 2009), which in turn are often one to one associated with NAL components in the UV. In the case of PKS 0558-504 we do not detect any intrinsic OVI or CIV absorption (see also Dunn et al., 2007). All this makes the identification of the detected absorber with a high velocity nuclear ionized outflow, unlikely.

A WA with unprecedented velocity, metallicity and ionization phases, appears to us to be less likely than the well-predicted WHIM possibility. We therefore tentatively identify this complex absorber with an intervening WHIM filament at the mean common redshift of $z = 0.118 \pm 0.001$, and in the following discussion associate the X-ray absorber with the

Far-UV BLB and BLA detected in the FUSE and IUE spectra.

5.2. Metallicity and Thickness of the WHIM Filament

In principle, the detection of clearly associated metal and HI transitions from the same WHIM filament, allows one to measure the the metallicity of the absorber. In our case, the spectral resolution of the X-ray data is much poorer than that of the superior quality FUSE data, and the best-fitting width of the HI BLB absorber tentatively identified at a redshift consistent with that of the X-ray absorber ($\text{FWHM}=160_{-30}^{+50} \text{ km s}^{-1}$), is narrower than the expected HI BLB thermal width in gas with the temperature inferred from teh X-ray data. Thus a direct association between the HI BLB and the OVIII absorbers cannot be clearly established, based on these data. However, both the redshifts of the HI BLB and the OVIII absorbers, and the thermal width of the HI BLB lines, are consistent, within the large uncertainties (e.g. Fig. 9), with the hypothesis that the bulk of the HI and the OVIII absorbers are imprinted by the same gas. Under this assumption, we then estimate the metallicity of the putative WHIM filament, and note that this estimate would translate in a lower limit if the BLB and the metal absorbers were structured or not one-to-one associated.

From the measured temperature, $\log T = 6.56_{-0.04}^{+0.19}$ we derive the relative fraction of HI compared to total H: $\xi_{HI} = (5.4_{-2.0}^{+0.5}) \times 10^{-8}$. As already mentioned in /S 3.3, the best-fitting temperature of the absorber is virtually independent on metallicity. We checked this by building two additional grids of models (other the one with $Z = Z_{\odot}$ used to fit the X-ray data) with metallicity of $Z = 0.1Z_{\odot}$ and $Z = 0.01Z_{\odot}$. Figure 12 shows the OVIII to HI fractional abundance ratio as a function of the temperature of the gas, for $Z = Z_{\odot}$ (black, solid curve), $Z = 0.1Z_{\odot}$ (red, solid curve) and $Z = 0.01Z_{\odot}$ (green, dashed curve). The ionization balance of the gas, at equilibrium, is virtually independent on the value of Z . From the metal-independent ionization correction value (i.e. $\xi_{HI} = (5.4_{-2.0}^{+0.5}) \times 10^{-8}$), and the intrinsic (i.e. at $z = 0.1183$) HI column of $N_{HI} = (9 \pm 2) \times 10^{13} \text{ cm}^{-2}$ (inferred from the measured $\text{EW}(\text{BLB}) = 66 \pm 16 \text{ m\AA}$ and $\text{FWHM}(\text{BLB}) = 160_{-30}^{+50} \text{ km s}^{-1}$), we can thus derive the expected equivalent H column density of the absorber, which turns out to be: $N_H = (1.7_{-0.4}^{+0.7}) \times 10^{21} \text{ cm}^{-2}$ (Table 3). Our best fitting WHIM model measures $N_H = (3.2_{-1.6}^{+3.1}) \times 10^{19} (Z/Z_{\odot})^{-1} \text{ cm}^{-2}$. This gives $Z/Z_{\odot} = 0.02_{-0.01}^{+0.02}$, or $Z = (1 - 4)\% Z_{\odot}$ (Table 3).

With an estimate of the equivalent hydrogen column density of the absorber in hand, we can estimate the thickness of the absorber along the line of sight. This is given, assuming homogeneity by the ratio between the column and the volume baryon densities of the absorber: $D = N_b/n_b$. The value of n_b is not constrained by the XMM-Newton data of PKS 0558-504.

However, hydrodynamical simulations that include feedback from galaxy super-winds predict that n_b in the WHIM correlates with temperature (e.g. Figure 3 in Cen & Ostriker, 2006), and that for a given temperature, lower metallicities are normally found in higher density environments (e.g. Figure 14 in Cen & Ostriker, 2006)¹⁵. From Fig. 14 of Cen & Ostriker (2006), at $T \sim 5 \times 10^6$ K, metallicities of the order of $\log(Z/Z_\odot) \simeq -1.5$ are reached at overdensities, compared to the average density of the Universe ($\langle n_b \rangle = 2 \times 10^{-7} (1+z)^3 (\Omega_b h^2 / 0.02)$) of $\delta = n_b / \langle n_b \rangle \simeq 300$ ¹⁶. At $z = 0.118$ and assuming $h = 0.7$, and $\Omega_b = 0.046$, this gives $n_b \simeq 10^{-4} \text{ cm}^{-3}$. This implies $D \simeq 5_{-1}^{+2} \times (n_b / \langle n_b \rangle)^{-1}$ Mpc.

Table 3 summarize the physical and geometrical parameters of the WHIM filament at $z = 0.118 \pm 0.001$, along the line of sight to PKS 0558-504.

5.3. Number Density and Cosmological Mass Density of WHIM

A tentative OVIII detection along a single line of sight cannot be used to measure the number density of OVIII filaments and the cosmological mass density in the WHIM. However, we think that, in this particular case, this exercise is instructive, because it clearly shows the serendipitous nature of the detection, and its bias toward dense (i.e. high equivalent width) and rare absorbers.

We estimate the number density of OVIII WHIM filaments, dN_{OVIII}/dz and Ω_b^{WHIM} , by taking into account the large Poissonian errors associated with small number statistics (Gehrels, 1986)¹⁷. We get: $dN_{OVIII}/dz = 7.3_{-6.6}^{+21.1}$ and $\Omega_b^{WHIM} = 0.18_{-0.16}^{+0.54}$ (90% significance). These numbers should be compared to the expected number density of WHIM filaments along a random line of sight, and to the total number of baryons as inferred by both microwave background anisotropies ($\Omega_b = 0.046 \pm 0.002$, Bennett et al., 2003; Spergel et al., 2003) and by the standard “big-bang nucleosynthesis” when combined with light-element

¹⁵This is because super-winds are very efficient in metal-polluting the IGM in the proximity of the host galaxy, but can only spread a finite amount of metals in a finite volume. Therefore IGM regions with lower primordial baryon densities will increase their gas metal content more than regions with initially higher baryon densities.

¹⁶This is consistent with our a-priori assumption of freezing the value of the baryon density to $n_b = 10^{-5} \text{ cm}^{-3}$ in our fit to the X-ray data, since at $n_b \geq 10^{-5} \text{ cm}^{-3}$ the contribution of photoionization is negligible, and the best-fitting temperature and column densities are not affected by the exact value of this parameter.

¹⁷We do not try to include systematics here, because of the already big (and probably dominating) statistical uncertainties associated with a single detection, which allow for the estimate to be consistent with all possible theoretical predictions.

ratios ($\Omega_b = 0.044 \pm 0.004$, Kirkman et al., 2003). From Cen & Fang (2006; their Figure 4), we derive $dN_{OVIII}/dz(EW > 9 \text{ m}\text{\AA}) \simeq 0.8$. This is consistent with the 90% significance lower limit of our estimate. Similarly, our estimate of $\Omega_b^{WHIM}/\Omega_b = 3.9_{-3.5}^{+11.7}$ greatly exceeds the expected value of about 40-50 % at $z \sim 0$ (e.g. CO06), but is consistent within the large 90% uncertainties. This is not surprising, since the WHIM detection we report is a serendipitous discovery in the spectrum of a target whose observations were not planned with this aim, and as such is biased toward dense (i.e. high equivalent width) and rare absorbers.

5.4. Caveats and their Solutions

Although the association between UV and X-ray absorbers reported here, makes this detection of a probable WHIM filament the first for which a metallicity measure is possible, we caution that, due to instrumental limitations and uncertainties, a definitive identification of this absorber with an intervening WHIM filament, is not possible with the current data.

First, the absorption that we identify here in X-ray as an OVIII Ly α at $z = 0.117 \pm 0.001$, could also, in principle be identified as OVII K β near the systemic redshift of PKS 0558-504. We reject this interpretation based on the non-detection of associated OVII K α absorption with the predicted strength ($\gtrsim 6$ times stronger than the detected line) - together with several other strong lines that should be detectable in the X-ray spectrum (CVI, NVI, NVII, NeIX, etc.) - and the lack of intrinsic OVI absorption in the RGS and FUSE spectra of PKS 0558-504, respectively. Moreover, the absorption seen both in FUSE and IUE and here identified as HI absorption cannot plausibly be identified with any transition at or near the systemic redshift of the target. Unfortunately, however, the OVII K α transition which would be associated with OVII K β at $z \simeq z_{sou}$, falls close to a strong RGS instrumental feature, which makes the source-frame absorption hypothesis difficult to reject with high confidence. The identification of the reported X-ray absorber with intrinsic nuclear OVII K β is thus unlikely, but not impossible based on the current X-ray data only. The only way of confirming the intervening origin of the X-ray absorber would be to clearly detect the other two lines predicted by the best-fitting WHIM model (one of which already hinted in the GO RGS1 and CAL RGS2 spectra of PKS 0558-504): i.e. FeXVII L($\lambda = 15.015 \text{ \AA}$) and NeIX K α , which fall at $\lambda = 15.02$ and $\lambda = 16.77 \text{ \AA}$. This is a task that only the *Chandra* LETG grating could accomplish, thanks to its 40 cm² effective area at this energies (vs $\sim 50 \text{ cm}^2$ for the RGS2 and $\sim 15 \text{ cm}^2$ for the *Chandra* MEG), and factor of ~ 2.5 better spectral resolution, compared to the RGS.

Second, while our identification of the absorber as a system at $z = 0.118 \pm 0.001$ is the most probable with the currently available data, its origin might not be intervening.

The absorber could also be intrinsic to the nuclear Seyfert environment, outflowing from the nucleus of PKS 0558-504. We discuss this possibility in §5.1, and conclude that the physical parameters inferred for this absorber, make this interpretation unlikely. A way to definitely exclude this possibility, is to look for variability of the X-ray and far-UV features reported here. Observations with the HST-COS of the far-UV spectrum of PKS 0558-504, would not only definitely confirm or rule out the existence of Ly α - β absorption at $z = 0.1183 \pm 0.0001$ (the redshift in FUSE), but would also test for opacity (i.e. ionization state and/or column density) variability of this absorber, which, if detected, would make the WHIM identification impossible. Analogously, new high S/N X-ray (*Chandra*) high-resolution spectra of PKS 0558-504 would allow one to check for variability of the X-ray absorber.

A third observation that can help shedding light on the true identification of this absorber, by either strongly supporting or weakening the support for its intervening nature, is a measure of the galaxy density in the region surrounding the putative WHIM filament at $z = 0.118$. WHIM filaments are supposed to correlate strongly with concentrations of galaxies and with Large Scale Structure (e.g. Stocke et al., 2006b). Unfortunately, the line of sight to PKS 0558-504 lies in the Southern sky, at a location which is currently poorly investigated: none of the major galaxy surveys or deep surveys (e.g. 2dF¹⁸, 6dF¹⁹, SDSS²⁰), covers this region of the sky. Wide-field, multi-band observations, centered on the line of sight to PKS 0558-504, and sensitive down to a fraction of L^* at $z = 0.118$, would allow photometric redshifts of the galaxies in the field to be determined with sufficient accuracy to exclude foreground and background objects. Spectroscopic follow-ups would then allow one to precisely estimate the galaxy density at $z = 0.118$ in a surrounding area around the line of sight to PKS 0558-504, to investigate on the association of WHIM filaments and LLSs.

6. Conclusions

We reported on the first combined and possibly associated Far-UV and X-ray tentative detection of a WHIM filament at a mean common redshift of $z = 0.118 \pm 0.001$, along the line of sight to the Seyfert PKS 0558-504. Our main findings are:

- OVIII Ly α absorption is tentatively identified at $z = 0.117 \pm 0.001$ in two independent

¹⁸<http://www.mso.anu.edu.au/2dFGRS/>

¹⁹<http://www.aao.gov.au/local/www/6df/>

²⁰<http://www.sdss.org/>

XMM-*Newton* RGS1 spectra of the Seyfert galaxy PKS 0558-504: a high S/N 480 ks net GO spectrum taken in 2008, and the sum of a number of much lower S/N spectra taken between 2000-2001 as part of an XMM-*Newton* calibration campaign, with a total net exposure of 309 ks. The combined, single-line significance of these two detections is 2.8σ .

- When fitted with a model including proper parameterizations of the continua together with our hybrid (collisional ionization plus photoionization) WHIM absorption model, the two full-band RGS1 and RGS2 spectra are consistent with the presence of a WHIM filament at $z = 0.117 \pm 0.001$ with $\log T = 6.56_{-0.17}^{+0.19}$ and $N_H = (3.2_{-1.6}^{+3.1}) \times 10^{19} (Z/Z_\odot)^{-1} \text{ cm}^{-2}$. Based on X-ray data only, the parameters of this model are poorly constrained and both represent only lower limits at a 3σ statistical confidence level.
- Archival FUSE data of PKS 0558-504 show the presence of a broad absorption complex at $\lambda = 1147.1 \pm 0.1$, with single-line statistical significance of 4.1σ (3.7σ when systematics are included). This line can be identified as broad HI Ly β at $z_{BLB} = (0.1183 \pm 0.0001)$, consistent with the redshift of the putative X-ray OVIII Ly α , within the large X-ray uncertainties. The width of this BLB absorber is marginally consistent, at a 2.5σ level, with the thermal width of HI ions in gas with $\log T = 6.56_{-0.17}^{+0.19}$ (the best-fit temperature derived from the X-ray data).
- Archival IUE-SWP, low-resolution, spectra of PKS 0558-504 taken in 1987 and 1989, also hint to the presence of an unresolved intervening HI Ly α at $z_{BLA} = 0.119 \pm 0.001$, with a single-line statistical significance of only 1.7σ . The redshift of this absorber is consistent, within their relative 1σ uncertainties, with the redshift z_{BLB} of the HI absorber detected with FUSE. The BLA (IUE) to BLB (FUSE) equivalent width ratio of these two lines, is consistent with the expected unsaturated value.
- We tentatively associate the OVIII Ly α X-ray absorber at $z = 0.117 \pm 0.001$, with the far-UV BLB and BLA absorbers at $z_{BLB} = (0.1183 \pm 0.0001)$ and $z_{BLA} = 0.119 \pm 0.001$, respectively, and identify them with an intervening WHIM filament at the mean common redshift of $z = 0.118 \pm 0.001$. The combined significance of this detection is 5.2σ (4.6σ if systematics in the FUSE continuum modeling are taken into account and the IUE HI BLA line is not considered).
- The above identification allows us to estimate for the first time the equivalent hydrogen column density of the absorber and so its metallicity under the assumption that the bulk of the HI BLB and the OVIII absorbers are physically associated. These turn out to be: $N_H = (1.5_{-0.4}^{+0.7}) \times 10^{21} \text{ cm}^{-2}$ and $Z = (1 - 4)\% Z_\odot$. If the HI BLB and the OVIII

absorbers are not directly associated or are structured, the above estimate represent upper and lower limits, respectively.

- The non-detection of associated OVI absorption in the FUSE spectrum of PKS 0558-504, allows us to put a stringent lower limit on the temperature of the absorber: by combining X-ray and FUSE data we obtain: $\log T = (6.56^{+0.19}_{-0.04})$ K.
- From the theoretical correlation between the temperature of WHIM filaments and their overdensity (relative to the average density in the Universe) and the expected 3D metallicity-temperature-overdensity relationship, we derive an overdensity of $\delta \sim 300$ for our system, and therefore a thickness along the line of sight of 5^{+2}_{-1} Mpc.
- Finally from this single detection we extrapolate the number density of OVIII Ly α WHIM absorbers, and the cosmological mass density of WHIM. Both are consistent, within their large 1σ uncertainties due to the low-number statistics, with the expected values, but their central-values are significantly higher due to the natural bias toward dense (i.e. high equivalent width) and rare absorbers associated with serendipitous WHIM detections.

FN, LZ and MLC acknowledge support from the LTSA grant NNG04GD49G. FN acknowledges support from the FP7-REGPOT-2007-1 EU grant No. 206469. This research has made use of the NASA/IPAC Extragalactic Database (NED) which is operated by the Jet Propulsion Laboratory, California Institute of Technology, under contract with the National Aeronautics and Space Administration.

REFERENCES

- Blustin, A.J., Page, M.J., Fuerst, S.V., Branduardi-Raymont, G., Ashton, C.E., 2005, *A&A*, 431, 111
- Brinkman, A.C., et al., 2000, *ApJ*, 530, L111B
- Buote, D.A., Zappacosta, L., Fang, T., Humphrey, P.J., Gastaldello, F., Tagliaferri, G., 2009, *ApJ*, 695, 1351
- Cen, R. & Fang, T., 2006, *ApJ*, 650, 573
- Cen, R. & Ostriker, J.P., 2006, *ApJ*, 650, 560: CO06
- Crenshaw, D.M., Kraemer, S.B. & George, I.M., 2003, in *Mass outflow in active galactic nuclei: new perspectives*, The Observatory, vol. 123, no. 1172, p. 57
- Danforth, C.W. & Shull, M.J., 2008, *ApJ*, 679, 194

- Danforth, C.W. & Shull, M.J., 2005, ApJ, 624, 555
- Dav, R., Cen, R., Ostriker, J.P., Bryan, G.L., Hernquist, L., Katz, N., Weinberg, D.H., Norman, M.L., O’Shea, B., 2001, ApJ, 552, 473
- den Herder, J.W. et al. 2001, A&A 365, L7
- Dunn, J.P., Crenshaw, D.M., Kraemer, S.B., Gabel, J.R., 2–7, AJ, 134, 1061
- Fang, T., Canizares, C.R., Yao, Y., 2007, ApJ, 670, 992
- Fields, D.L., Mathur., S., Krongold, Y., Williams, R., Nicastro, F., 2007, ApJ, 666, 828
- Fields, D.L., Mathur., S., Pogge, R.W., S., Nicastro, F., Komossa, S., Krongold, 2005, ApJ, 634, 928
- Freeman, P.E., Doe, S. & Siemiginowska, A., 2001, SPIE Proceedings, Vol. 4477, p.76
- Fukugita, 2003, astro-ph/0312517
- George, I.M., Turner, T. J., Netzer, H., Nandra, K., Mushotzky, R.F., Yaqoob, T., 1998, ApJS, 114, 73
- Kaastra, J.S., Werner, N., den Herder, J.W.A., Paerels, F.B.S., de Plaa, J., Rasmussen, A.P., de Vries, C.P., 2006, ApJ, 652, 189: K06
- Kriss, G.A., 2002, in *Mass outflow in active galactic nuclei: new perspectives*, ASP Conference Proceedings, Vol. 255. Edited by D.M. Crenshaw, S.B. Kraemer, and I.M. George, San Francisco: Astronomical Society of the Pacific, 2002., p.69
- Krongold, Y. et al., 2009, ApJ, 690, 773
- Krongold, Y., Nicastro, F., Elvis, M., Brickhouse, N.S., Mathur, S., Zezas, A., 2005, ApJ, 620, 165
- Krongold, Y., Nicastro, F., Brickhouse, N.S., Elvis, M., Liedahl, D.A., Mathur, S., 2003, ApJ, 597, 832
- Nicastro, F., Mathur, S. & Elvis, M., 2008, Science, 319, 55 Nicastro, F. et al., 2005a, Nature, 433, 495
- Nicastro, F. et al., 2005b, ApJ, 629, 700
- Papadakis, I. et al., 2009, A&A, submitted
- Piconcelli, E., et al., 2005, A&A, 432, 15
- Shull, J.M., 2003, in *The IGM-Galaxy Connection*, Eds. Rosenberg, J.L. & Putman, M.E., Kluwer Academic Publishers, Dordrecht, vol. 281, 1
- Rasmussen, A.P., Kahn, S.M., Paerels, F.; den Herder, J.W., Kaastra, J., de Vries, C., 2007, ApJ, 656, 129: R07
- Reeves, J.N. et al., 2009, ApJ, 701, 493
- Savage, B.D. et al., 2003, ApJS, 146, 125
- Sembach, K.R., Tripp, T.M., Savage, B.D., Richter, P., 2004, ApJS, 155, 351
- Sembach, K.R. et al., 2003, ApJS, 146, 165
- Shull, J.M., Stocke, J.T., Penton, S., 1996, AJ, 111, 72
- Stocke, J.T., Shull, J.M., & Penton, S.V., 2006a, Planets to cosmology : essential science in

the final years of the Hubble Space Telescope, Proceedings of the Space Telescope Science Institute Symposium. Edited by Mario Livio and Stefano Casertano. Cambridge, UK: Cambridge University Press, 2006. Space Telescope Science Institute symposium series, Vol. 18. ISBN 0-521-84758-3

Stocke, J.T., Penton, S.V., Danforth, C.W., Shull, J.M., Tumlinson, J., McLin, K.M., 2006b, ApJ, 641, 217

Tripp, T.M., Sembach, K.R., Bowen, D.V., Savage, B.D., Jenkins, E.B., Lehner, N.; Richter, P., 2008, ApJS, 177, 39

Uttley, P., 2009, proceedings of “High Resolution X-ray Spectroscopy: Towards IXO, Proceedings of the international workshop” held at the Mullard Space Science Laboratory of University College London, Holmbury St Mary, Dorking, Surrey, UK, March 19 - 20, 2009, Ed.s Branduardi-Raymont, G. and Blustin, A., published electronically at <http://www.mssl.ucl.ac.uk/~ajb/works>

p.E45 Wakker, B.P., 2006, ApJS, 163, 282

Yoshikawa, K. et al., 2003, PASJ, 55, 879

Table 1: Log of the XMM-Newton, FUSE and IUE Observations

Dataset	Date of Obs.	Obs. ID	Exposure ^a
XMM-RGS CAL	2000/02/07	0116700301 ^b	19.0
	2000/02/10	0117500201	40.8
	2000/02/12	0117710701	49.9
	2000/02/13	0117710601	56.9
	2000/02/14	0117710501	6.8
	2000/03/07	0120300501	6.5
	2000/03/07	0120300601	7.0
	2000/03/07	0120300801	39.7
	2000/05/24	0125110101	30.0
	2000/10/10	0129360201	26.4
	2001/06/26	0137550201	14.8
	2001/10/19	0137550601	14.6
	XMM-RGS GO	2008/09/07	0555170201
2008/09/09		0555170301	127.8
2008/09/11		0555170401	126.2
2008/09/13		0555170501	126.6
2008/09/13		0555170601	115.8
FUSE-LWRS	1999/12/10	P1011504000	46.2
	2002/11/07	C1490601000	48.3
IUE-SWP LR	1987/09/22	SWP31899	13.8
	1989/11/14	SWP37589	13.8
	1989/11/15	SWP37604	16.2

^a Net, in ksec. ^b RGS1 only.

Table 2: Absorption Lines (and upper limits) in the XMM-Newton RGS, FUSE and IUE spectra of PKS 0558-504

Wavelength in Å	Width FWHM in km s ⁻¹	EW in mÅ	Significance in σ	Id	Redshift in km s ⁻¹ if $z < 10^{-3}$
XMM-Newton RGS					
23.52 ± 0.03	< 900	$23.7^{+5.0}_{-3.7}$	6.4	OI _{Kα}	± 380 km s ⁻¹
21.61 ± 0.03	< 900	12.9 ± 5.2	2.5	OVI _{Kα}	138 ± 380 km s ⁻¹
21.17 ± 0.03	< 1200	9.1 ± 3.3	2.8	OVI _{Kα}	0.116 ± 0.002
$15.00-15.03^a$	< 900 (fixed)	< 3.0	1 ^b	NeIX _{Kα}	0.117 ± 0.001
$16.76-16.79^a$	< 900 (fixed)	< 5.0	1 ^b	FeXVII _L	0.117 ± 0.001
FUSE-LWRS					
1147.1 ± 0.1	160^{+50}_{-30}	66 ± 16	4.1	HI _{Lyβ}	0.1183 ± 0.0001
$1152.7-1154.7^a$	50 (fixed)	< 12	1 ^b	OVI($\lambda = 1031.9$)	0.118 ± 0.001
IUE-SWP LR					
1360 ± 1	< 1300	1000 ± 600	1.7	HI _{Lyα}	0.119 ± 0.001

^a Wavelength interval over which the 1σ EW upper limit is computed, corresponding to $z = 0.117 \pm 0.001$ for the X-ray lines, and $z = 0.118 \pm 0.001$ for the UV line.

^b 1σ upper limit.

Table 3: Physical and Geometrical Parameters of the WHIM Filament at $z = 0.118 \pm 0.001$

Redshift	log(T) (T in K)	N_H (in 10^{21} cm ⁻²)	Metallicity	Thickness ^a in Mpc
0.118 ± 0.001	$6.56^{+0.19}_{-0.04}$	$1.5^{+0.7}_{-0.4}$	(1-5) % Z_\odot	5^{+2}_{-1}

^a For a baryon volume density of $n_b = 10^{-4}$ cm⁻³.

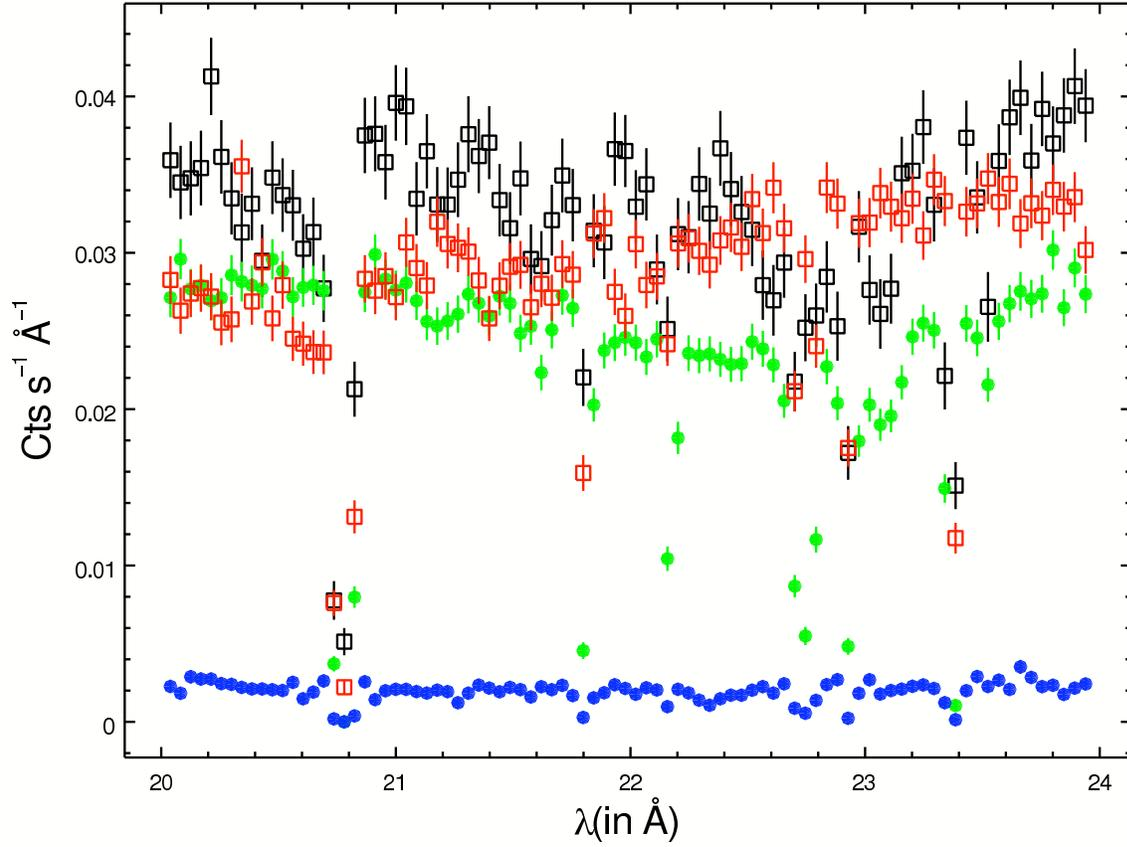


Fig. 1.— 20–24 Å portion of the RGS1 CAL (empty squares) and GO (filled circles) source (black and green, respectively) and background (red and blue, respectively) spectra of PKS 0558-504. The average background level during the CAL observations is about 10 times higher than that of the GO observations.

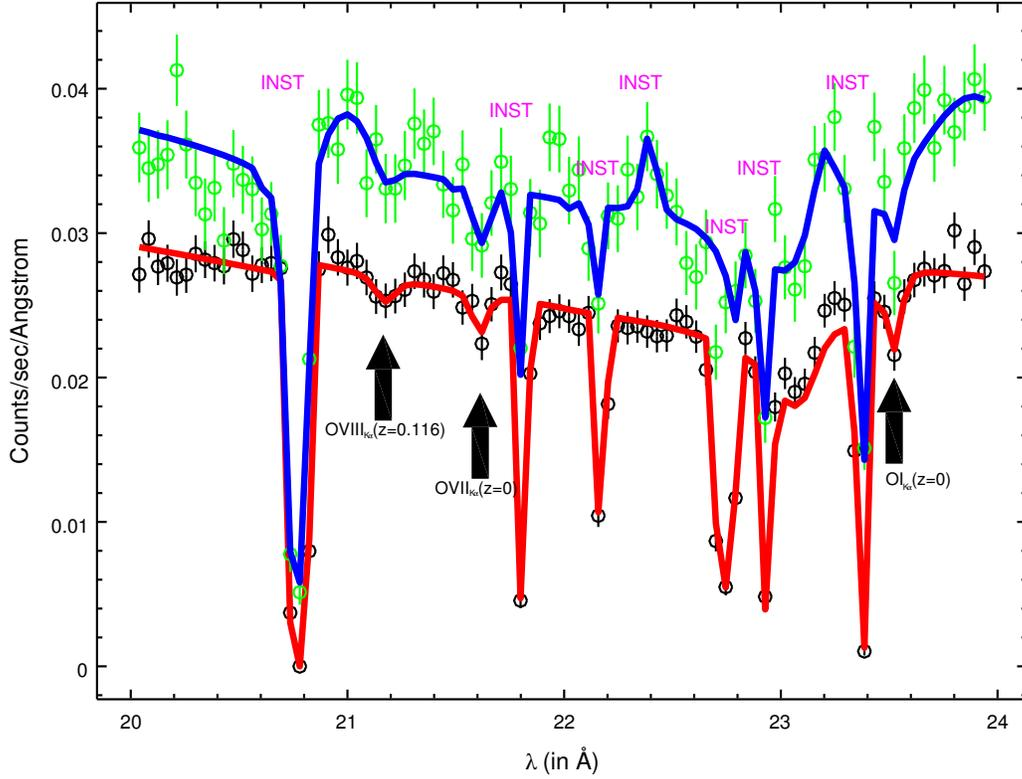


Fig. 2.— 20-24 Å portion of the CAL (green points and errorbars) and GO (black points and errorbars) RGS1 spectra of PKS 0558-504, along with their best fitting continuum plus absorption models. The deep line-like features present in both spectra are instrumental features, due to bad-pixels/columns of the read out CCD. The remaining three real features present in both spectra are marked and here identified as OI $K\alpha$ and OVII $K\alpha$ at $z \simeq 0$, and, tentatively, as OVIII $Ly\alpha$ at $z = 0.116 \pm 0.002$.

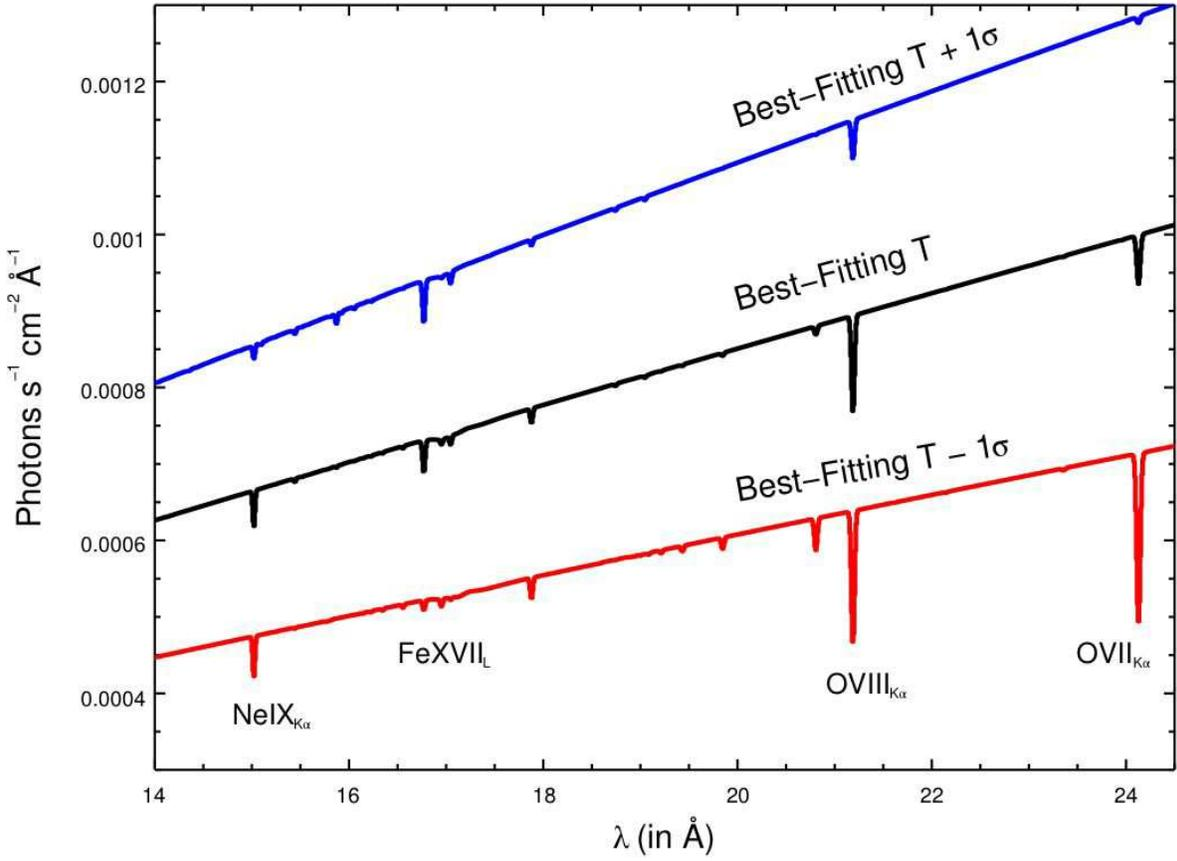


Fig. 3.— Best fitting WHIM model (black curve) together with its negative (red curve) and positive (blue curve) 1σ temperature indeterminations.

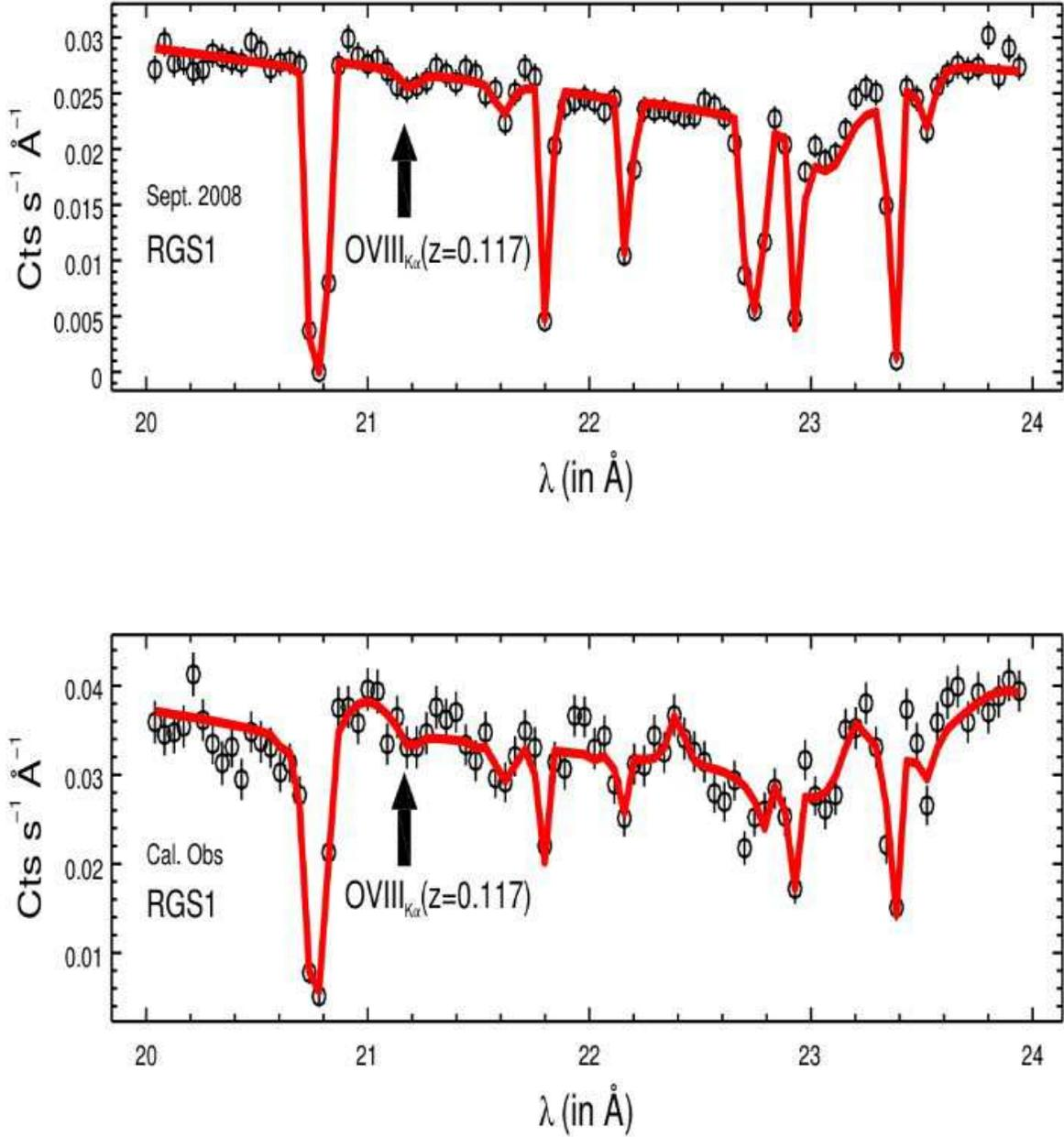


Fig. 4.— 21–24 \AA portion of the RGS1 GO (top panel) and CAL (bottom panel) spectra of PKS 0558–504. The superimposed red curve is the best fitting WHIM model convolved with the instrumental responses.

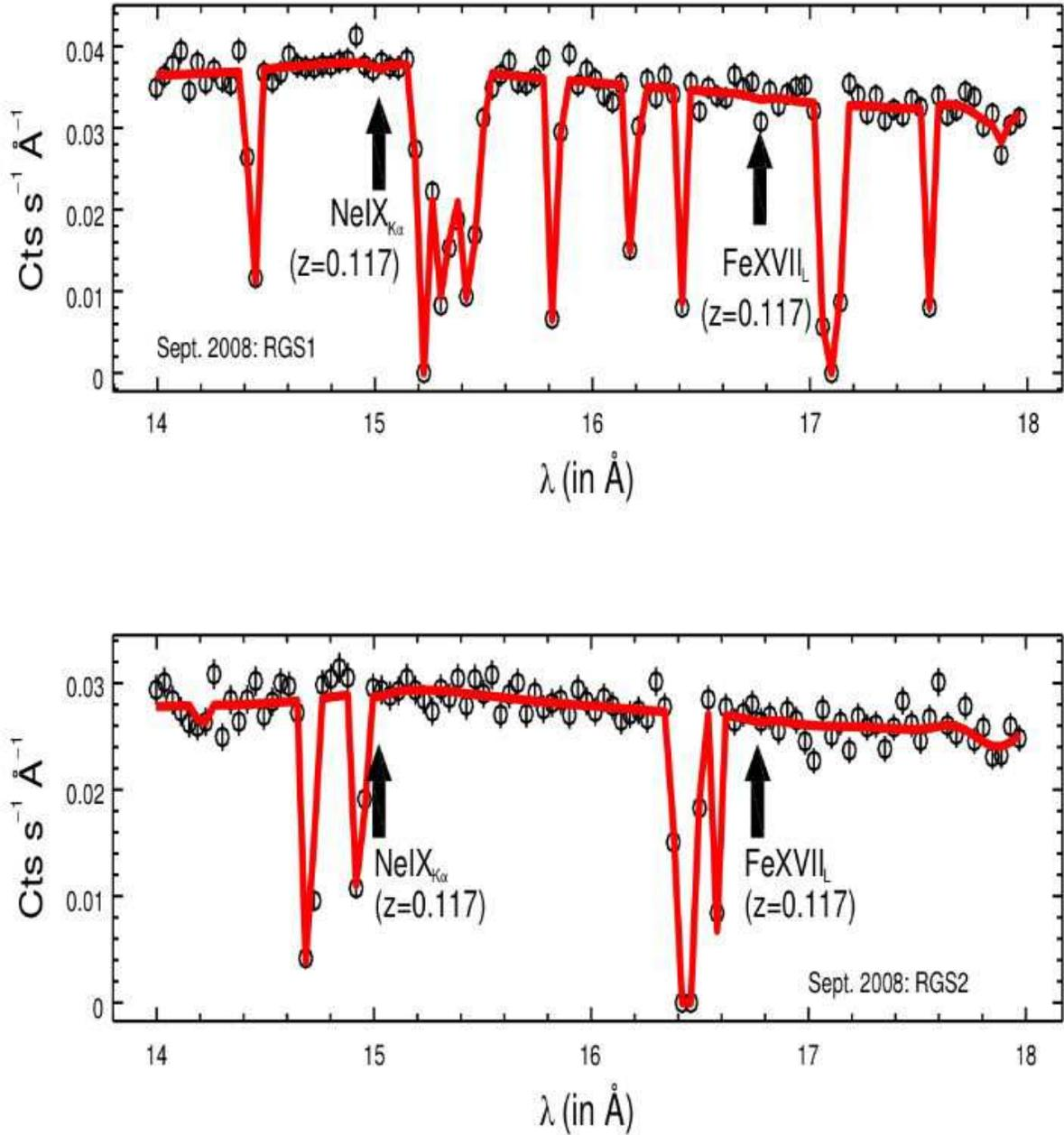


Fig. 5.— 14-18 \AA portion of the RGS1 (top panel) and RGS2 (bottom panel) GO spectra of PKS 0558-504. The superimposed red curve is the best fitting WHIM model convolved with the instrumental responses.

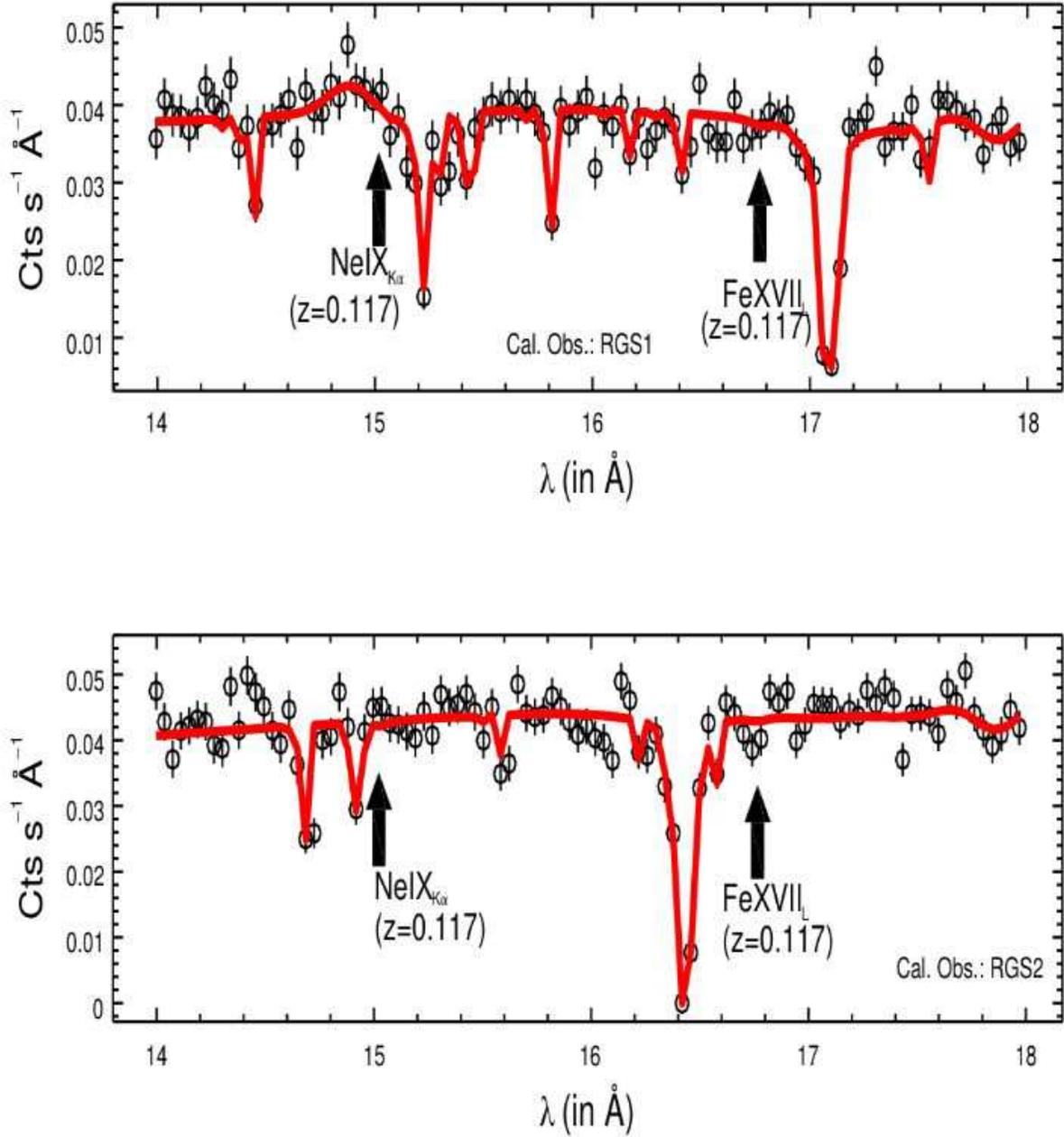


Fig. 6.— 14-18 \AA portion of the RGS1 (top panel) and RGS2 (bottom panel) CAL spectra of PKS 0558-504. The superimposed red curve is the best fitting WHIM model convolved with the instrumental responses.

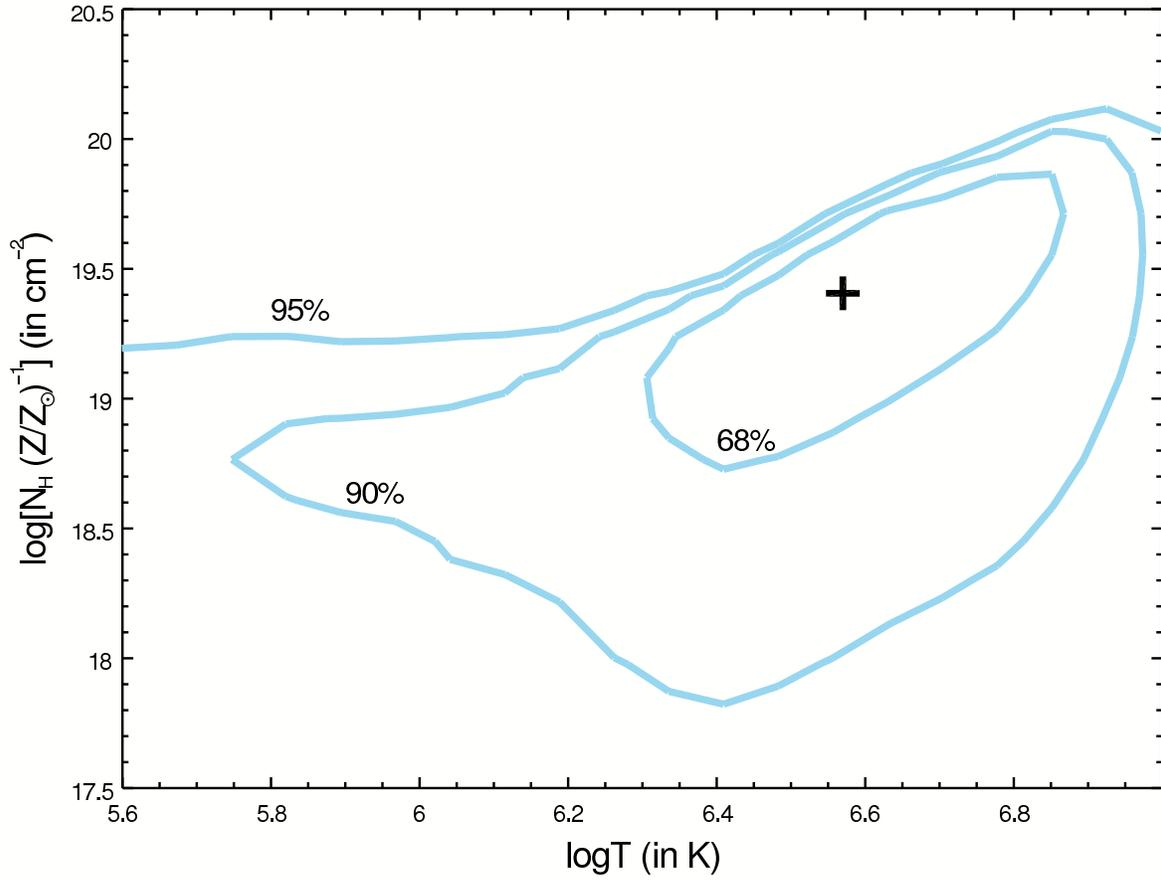


Fig. 7.— 68%, 90% and 95% $\log T$ - $\log N_H$ contours for the putative X-ray WHIM filament at $z = 0.117 \pm 0.001$

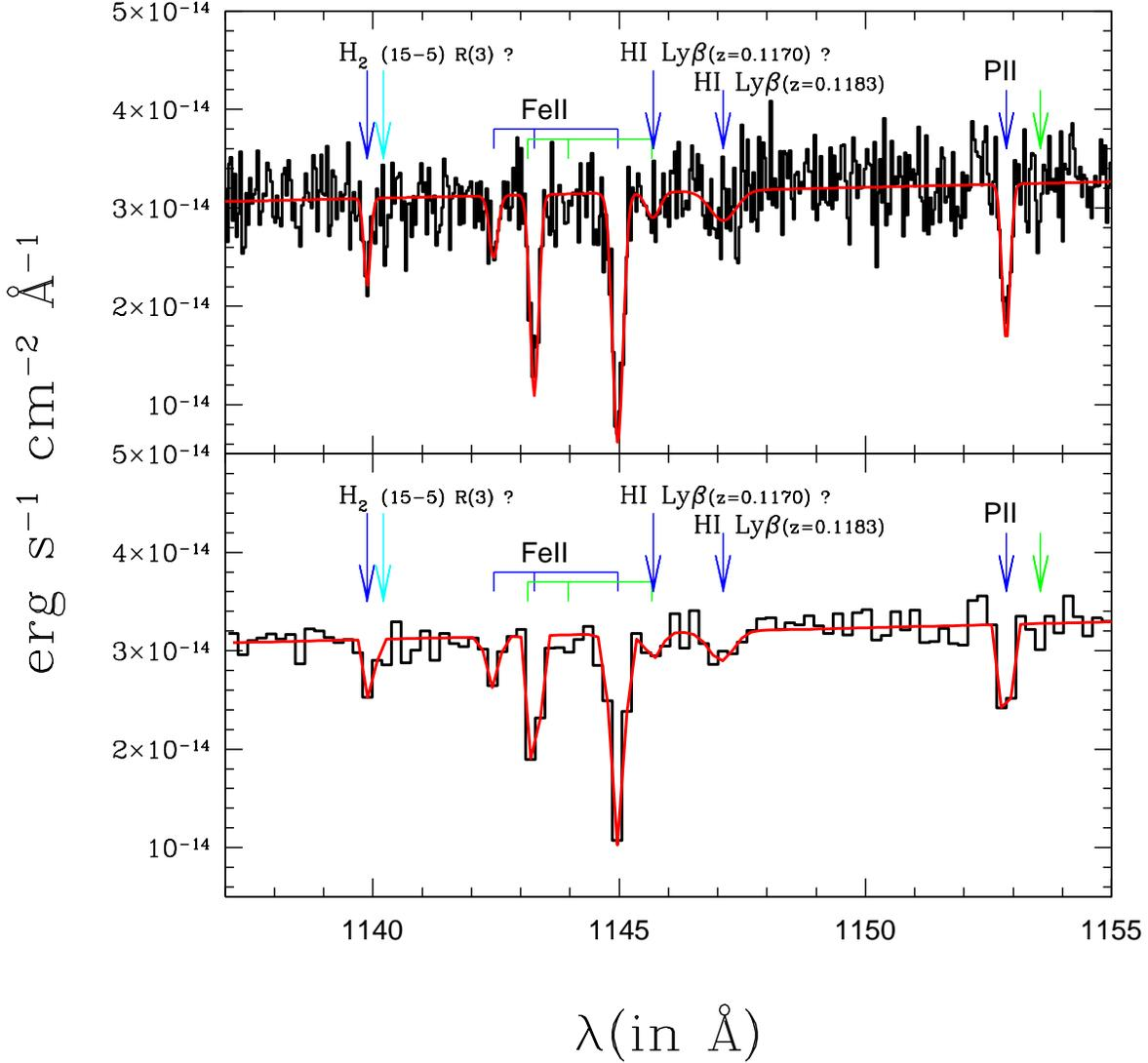


Fig. 8.— 1137-1155 \AA portion of the FUSE spectrum of PKS 0558-504, in two different binning schemes: $\sim 15 \text{ km s}^{-1}$, the FUSE resolution (top panel), and $\sim 90 \text{ km s}^{-1}$ (bottom panel). Absorption lines identifications are labeled in both panels. Low- and high-velocity components of the low-ionization Fe and P and molecular H_2 absorbers are marked in blue and green and blue and cyan, respectively, but only the much stronger low-velocity lines are fitted (with the exception of the high-velocity FeII($\lambda 1144.94$) line at $\lambda = 1145.7 \text{ \AA}$, which we fit because possibly partly contaminated by intervening HI absorption). The broad absorption complex that we tentatively identify as intervening HI Ly β is clearly better seen in the heavily binned spectrum (bottom panel).

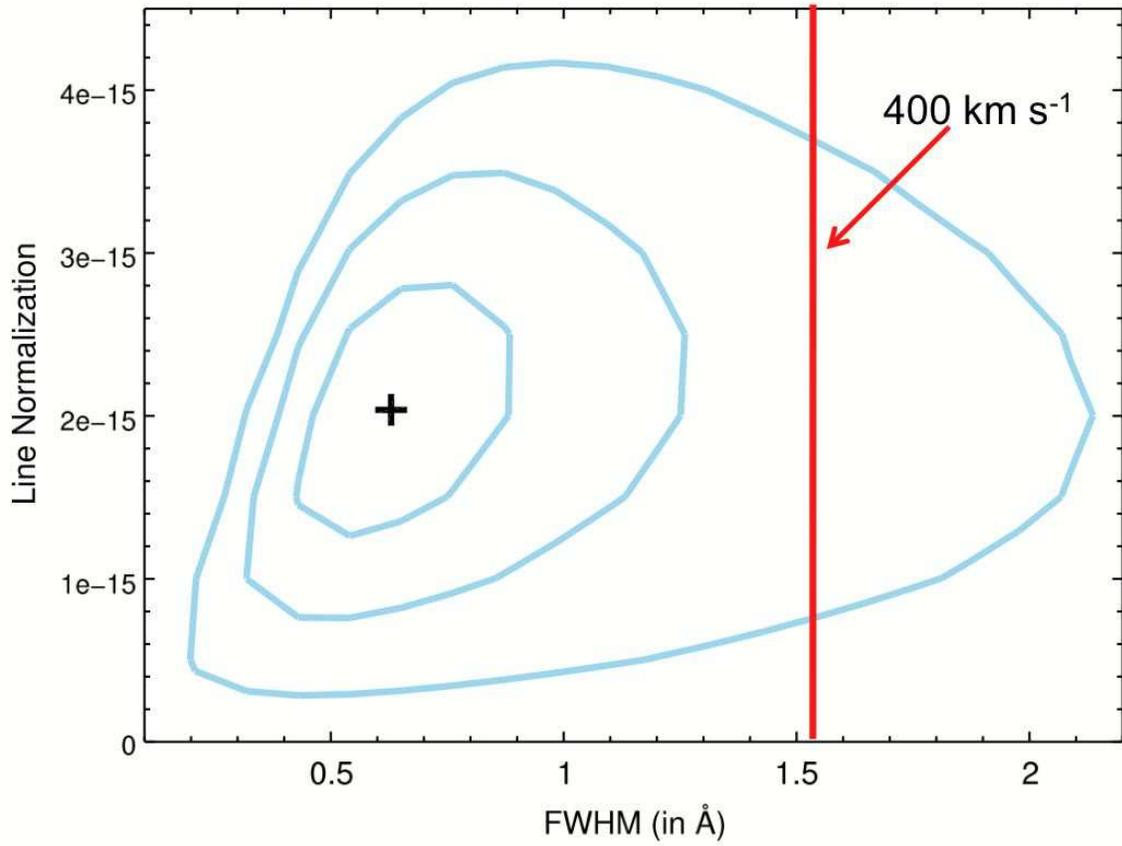


Fig. 9.— Gaussian normalization and FWHM 1, 2 and 3σ contour plot, for the $z_2 = (0.1183 \pm 0.0001)$ HI Ly β absorber. FWHM=1.5 Å corresponds to $v = 390 \text{ km s}^{-1}$ at $\lambda = 1147.1 \text{ Å}$, and so to the expected doppler parameter of $b \simeq 165 \text{ km s}^{-1}$, for hydrogen in gas at $\log T \sim 6.5$.

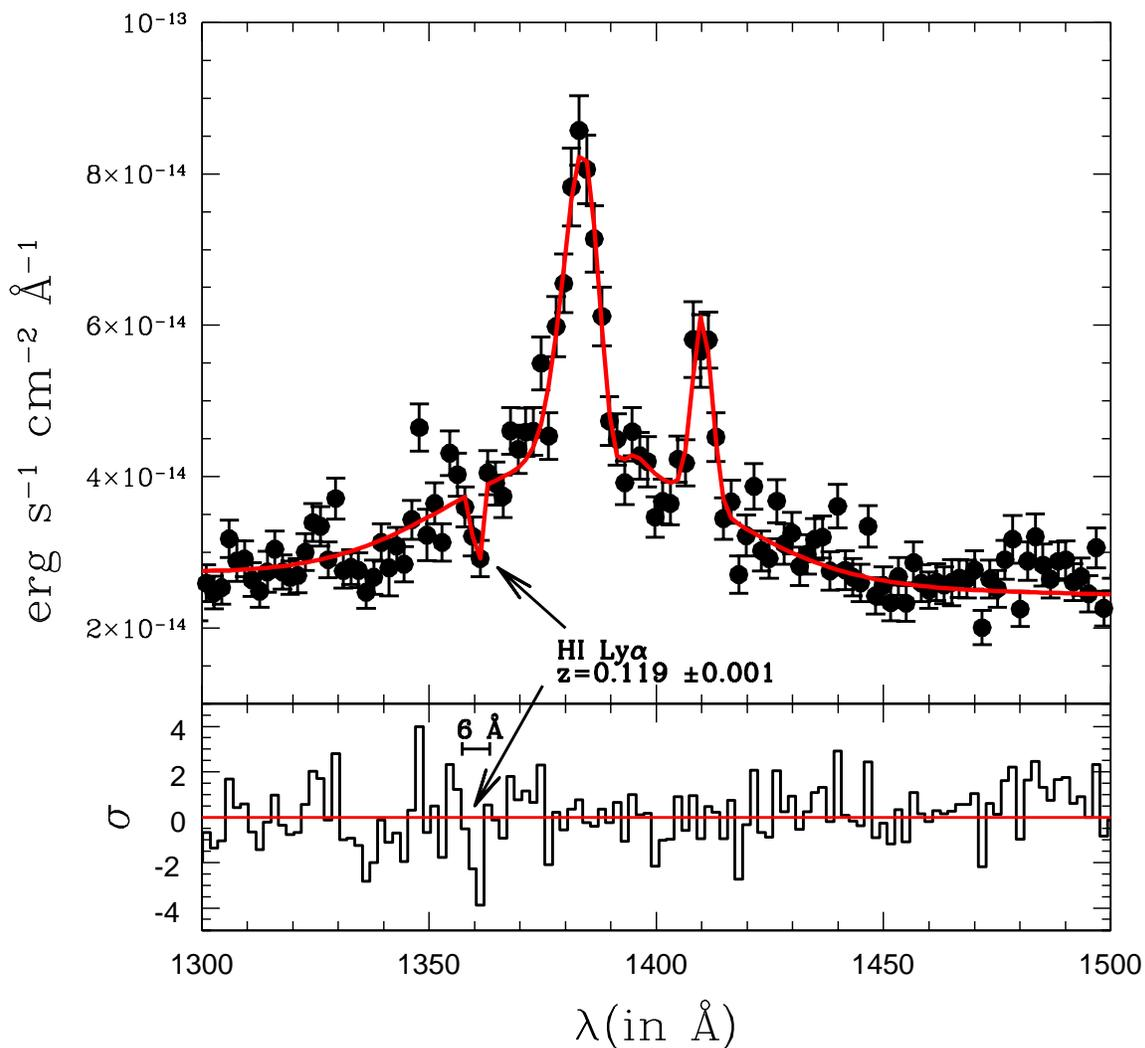


Fig. 10.— 1300-1500 \AA portion of the 1989, November 15 IUE-SWP LR spectrum of PKS 0558-504 (obsid 37604, Table 1) with our best-fitting superimposed (top panel), and the residuals after subtracting the Gaussian at $\lambda = 1360 \pm 1 \text{\AA}$ (bottom panel). Our tentative identification of a HI Ly α absorber at $z = 0.119 \pm 0.001$, is labeled.

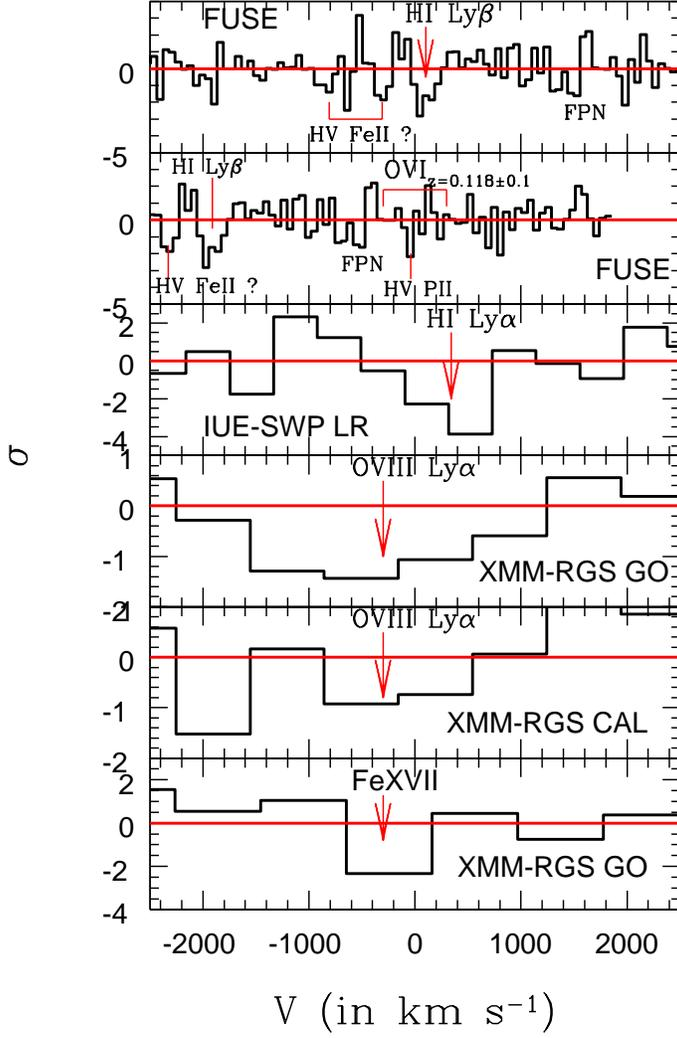


Fig. 11.— Residuals (in σ), in velocity space, to the best fitting continuum (plus ISM low-velocity lines, in the case of FUSE) models to the FUSE (first and second panel from the top), IUE-SWP LR (1989; third panel from the top) and XMM-*Newton* (GO: 4rd and 6th panels from the top; CAL: 5th panel from the top) spectra of PKS 0558-504. The residuals are centered around the absorption lines that we identify as HI Ly β , HI Ly α , OVIII Ly α and FeXVII L ($\lambda = 15.015 \text{ \AA}$, rest frame), at a mean common redshift of $z = 0.118 \pm 0.001$. The red arrows in the figures indicate the best-fitting centroid of each line in their respective spectra. The red segment labeled “OVI $_{z=0.118\pm 0.001}$ ” in the second panel from the top, mark the spectral region where OVI associated with the HI BLB is expected, and not seen. The feature labeled “FPN” (Fixed Pattern Noise) in the first and second panel from the top, is a known FUSE Lif2A segment instrumental feature (e.g. Sembach et al., 2004)

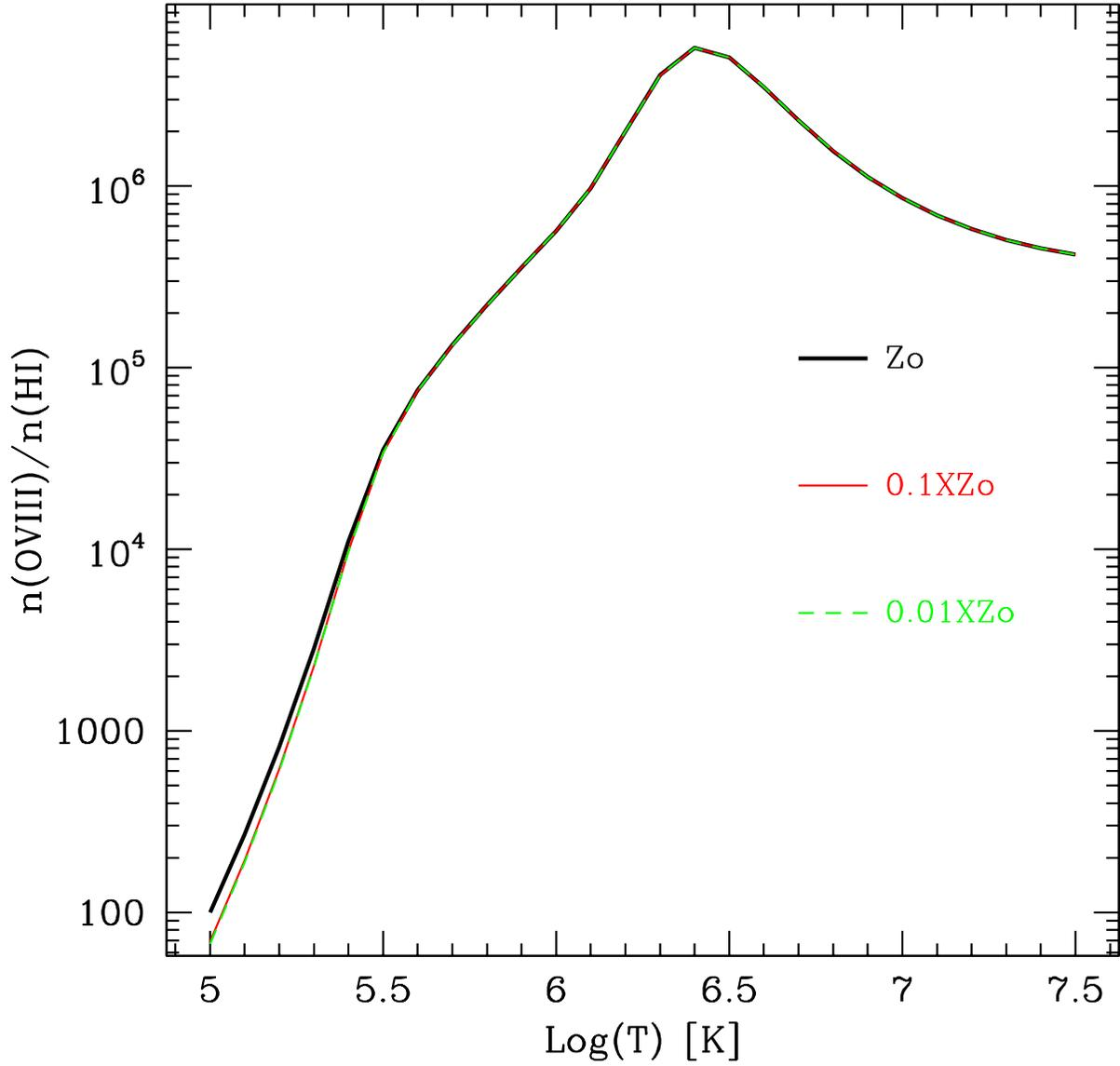


Fig. 12.— OVIII to HI fractional abundance ratio (i.e. ionization correction) as a function of the temperature of the gas, for three different absolute metallicities: $Z = Z_{\odot}$ (black solid curve), $Z = 0.1Z_{\odot}$ (red solid curve) and $Z = 0.01Z_{\odot}$ (green dashed curve). The ionization balance of the gas, at equilibrium, is virtually independent on the value of Z , and so is the ionization correction.